Effects of polyethylene glycol (PEG) on the corrosion inhibition of mild steel by cerium nitrate in chloride solution

H. Boudellioua, Y. Hamlaoui, L. Tifouti, F. Pedraza

Effects of Polyethylene Glycol (PEG) on the Corrosion Inhibition of Mild Steel by Cerium Nitrate in Chloride Solution

H. Boudellioua[1], Y. Hamlaoui[2], L. Tifouti[1], F. Pedraza[3*]

1. Laboratoire de Génie de l'Environnement (LGE), Université Badji Mokhtar, BP 1223, 23020 El Hadjar-Annaba, Algérie
2. Laboratoire de Physique de la Matière et Rayonnement (LPMR), Faculté des Sciences et de Technologie, Université Mohamed Chérif Messaadia, BP 1553, 41000 Souk-Ahras, Algérie
3. Laboratoire des Sciences de l'Ingénieur pour l'Environnement (LaSIE, UMR-CNRS 7356), Université de La Rochelle, Avenue Michel Crépeau, 17042 La Rochelle Cedex 1, France.

*Corresponding author: fpedraza@univ-lr.fr

Abstract

In this study, cerium was investigated as an inhibitor to improve the corrosion resistance of ASTM A915 mild steel in 0.1M NaCl solution. Increasing the Ce^{3+} concentration up to an optimum level of 600 $mg.L^{-1}$ (or 1.4 10^{-3} M) sharply decreased the corrosion rate (I_{corr}). However, the beneficial effect of cerium was lost after short immersion times at room temperature. In contrast, the addition of polyethylene glycol (PEG) to the cerium nitrate containing NaCl solutions enhanced protection through the formation of stable corrosion products and the decrease of cracks in the film formed on the surface of mild steel.

Keywords: Mild steel; Rare earth elements; Corrosion inhibition; Polarization; Electrochemical Impedance Spectroscopy; Materials Characterization.

1. Introduction

Mild steels are among the main construction materials widely employed in industry **[1]**. However, they are thermodynamically unstable when exposed to corrosive environments. In particular, localized corrosion occurs in the presence of halide ions **[2]**. One well-known approach to protect materials is the use of corrosion inhibitors, among which hexavalent chromium is particularly effective to prevent corrosion **[3]**. Cr(VI) compounds were banned in Europe already in 2007 and will be soon worldwide due to their highly carcinogenic and toxicity effects **[4-5]**. In this regard, cerium nitrate inhibitors are considered as an alternative solution to use for different metals and alloys **[6-9]**.

Already in 1989, Hinton *et al.* **[10]** demonstrated that the addition of cerium salts in aggressive environments reduced the corrosion of zinc and hindered the cathodic reaction of oxygen reduction. Ever since, different studies have focused on the use of cerium nitrate either as inhibitors on steel **[11]** or as electrodeposited coatings **[12, 13]**. As a corrosion inhibitor, cerium nitrate does not stop effectively the development of the corrosion products for prolonged immersion times **[14]**. In addition, the combination of hydroxide peroxide (H_2O_2) with cerium-based salts favours the precipitation of cerium oxide/hydroxide on the steel surface to result in coatings with enhanced corrosion resistance **[15]** but the use of H_2O_2 is also restricted.

Therefore, the introduction of polymers -like polyethylene glycol (PEG)- as corrosion inhibitors for metals in aggressive media has been proven to reduce corrosion of carbon steel in solutions of sulfuric and hydrochloric acids by increasing the resistance to pitting **[16-17]**. The beneficial effect of PEG is often associated with its adsorption at the surface of steel, thus blocking/limiting the physical contact between the corroding species and the steel **[18]**. Therefore, a shift to more positive potentials and a decrease of the anodic slope compared to the blank solution allow an improvement of the corrosion resistance **[19]**. In addition, Hamlaoui *et al.* **[20-21]** demonstrated that the incorporation of PEG to the electrodeposited ceria-based coatings led to a decrease in the number of cracks of the surface layers and provided enhanced corrosion protection on galvanized steel in NaCl and Na_2SO_4 media. However, little is known on the combined effects of cerium and PEG to improve the corrosion resistance of mild steel. Therefore, this paper intends to unveil the corrosion mechanisms and the optimal cerium concentration as inhibitor at room temperature and to investigate the combined effects of cerium and PEG on mild steel exposed to 0.1M NaCl solution for 30 days.

2. Experimental

2. 1. Materials and solution preparation

The chemical composition of mild steel (ASTM A915) used in present work is given in **Table 1**. The steel samples were cut from a bar with a diameter of 1 cm. A copper wire was welded to the back side and the whole embedded in epoxy resin leaving an exposed area of 0.95 cm^2 (i.e. the edges of the samples were not exposed). Thereafter, the samples were abraded with SiC emery paper until P4000, washed with distilled water, degreased with ethanol, rinsed again with distilled water to remove ethanol traces, and finally dried with hot air. This preparation step was carried out immediately before immersion of the samples in the solutions. In previous works **[22-24]** showed that decreasing NaCl concentration (especially in the case of EIS) results in more detailed information about the corrosion process. Therefore, the corrosion tests were carried out in 0.1M NaCl solutions (pH = 6.5) at room temperature (25 °C). The solutions were gently stirred to obtain a slight vortex of the electrolyte to aerate naturally the solutions.

The inhibitors were directly dissolved in the corrosive medium. The concentration of cerium nitrate, $Ce(NO_3)_3,6H_2O$ (Sigma-Aldrich, Mw = 434.22; 99.9%) was increased from 50 to 600 $mg.L^{-1}$, while a fixed concentration of Polyethylene Glycol (PEG) (Sigma-Aldrich, Mw = 1500 g/mol) of 2.5 $g.L^{-1}$ **[25]** was employed with the optimal concentration of cerium nitrate.

2.2. Electrochemical measurements

The electrochemical experimental set-up was composed of a classic three electrodes cell using a platinum wire as counter electrode (CE) surmounted with a saturated calomel electrode (SCE) as the reference one, and mild steel sample as working electrode (WE). The electrochemical measurements were performed using a PGZ 301 (Voltalab 40 model) potentiostat/galvanostat coupled to a frequency response analyzer (FRA) Volta Master IV software. The working electrodes were immersed in the aerated 0.1M NaCl solution with and without additions of cerium nitrate. The potentiodynamic polarization curves were obtained by using a sweep rate of 0.5 $mV.s^{-1}$ (or 30 $mV.min^{-1}$) between ±250 mV compared to the corrosion potential (E_{corr}). The resistance polarization values (R_p) were obtained between ±20 mV around the corrosion potential (E_{corr}), and at 0.167 $mV.s^{-1}$ of scan rate. The impedance data were obtained at the corrosion potential (E_{corr}) between 100 KHz and 5 mHz, with 4 mV as the applied sinusoidal perturbation. The EIS response from the samples was fitted using Z_{View} software. All the corrosion tests were repeated several times for reproducibility purposes.

2.3. Morphology and characterization of the films

The morphology of the surface was firstly investigated by optical microscopy and then analyzed more thoroughly by a field emission environmental microscope (FE-SEM) of FEI Quanta 200F coupled to an X-ray energy dispersive spectroscopy (EDS) using an EDAX detector to study the local composition of films. The Raman spectra were recorded with a Jobin-Yvon LabRam HR8000 spectrometer equipped with a confocal microscope using an incident monochromatic beam of 632.82 nm emitted by an He-Ne laser. The X-ray patterns were obtained in a Bruker AXS D8-Advanced diffractometer using Cu Kα radiation (α=0.15406 nm) at a scan rate of 0.04 s^{-1} in the symmetric configuration.

3. Results and discussion

3. 1. Concentration effect of cerium nitrate

3.1.1. Open circuit potential (OCP) and Polarization behavior

The open circuit potentials (OCP) of mild steel were recorded as a function of the immersion time over a period of 60 minutes in neutral 0.1M NaCl solution with and without various concentrations of cerium nitrate inhibitor until 600 $mg.L^{-1}$ (**Fig.1a**). Irrespective of the concentration, all the curves displayed a similar trend, where the potential rapidly moved towards more cathodic values at the beginning of the immersion and then tended to stabilize with time. The increase of cerium nitrate inhibitor concentrations (from 50 to 600 $mg.L^{-1}$) shifted the OCP towards more negative values and stabilized more rapidly than without inhibitor. This stabilization phenomenon can be ascribed to the formation and stabilization of the electrical double layer, and/or to the deposition of cerium layer at the surface that limited the transport of oxygen to the steel surface and decreased the oxygen reduction reaction **[26]**.

Fig.1b shows the polarization curves of mild steel samples immersed in 0.1M NaCl solution with and without cerium nitrate obtained after 30 minutes of immersion time at various concentrations and room temperature. As with **Fig.1a**, the corrosion potential was shifted towards more cathodic values with increasing the concentration of cerium nitrate in the NaCl solution. In addition, the cathodic slopes decreased thereby suggesting that cerium nitrate performed as a cathodic inhibitor. According to the shape and to the βc cathodic values of the polarization curves, the corrosion rate in the aerated NaCl solution with cerium nitrate appeared under cathodic control (oxygen diffusion) when compared to the curve obtained from the blank in 0.1M NaCl solution. K. Aramaki proved that the cerium species -and not the counter anions (chlorides and nitrates)- were the sole responsible in changing the reduction reactions **[27]**. Also, Hosseini *et al.* **[28]** demonstrated that a film of cerium hydroxides or of hydrated oxides

formed on the surface of the substrate when immersed in NaCl. Such film hindered the diffusion of oxygen and slowed down the cathodic reaction. The same conclusions were drawn by B.R.W. Hinton, who reported that the increase of interfacial pH that brings about the precipitation of cerium oxides/hydroxides on the cathodic sites **[29,30]**. Majdi *et al*. also showed that the higher the local pH, the faster the nucleation rate of cerium oxide particles **[31]**.

To verify such hypotheses, the corrosion parameters E_{corr}, I_{corr} and R_p were calculated in the vicinity of the open circuit potential using the Stern-Geary method $\mathbf{I_{corr} = \frac{\beta a}{2.3\ Rp}}$, or/and $I_{corr} = \frac{1}{2.3\ Rp}\frac{(\beta a.\beta c)}{(\beta a+\beta c)}$ (the second one was used mainly for free mild steel) **[32]**; where βa and βc are the anodic and cathodic Tafel slopes in (mV/decade) and (mV), respectively, and R_p is the polarization resistance (**Table 2**). The inhibition efficiency (IE %) given in **Tables 2, 4** and **6** was calculated using the conventional equation: **IE (%) = 100 x (I^0_{corr} - I_{corr})/ I^0_{corr}**, where I^0_{corr} and I_{corr} are the corrosion current densities for untreated and treated bare mild steel, respectively.

It was observed (**Table 2**) that the corrosion rate values (I_{corr}) decreased with increasing the concentration of cerium nitrate until the value I_{corr} = 4.59 µA/cm^2 at 600 mg.L^{-1} (with IE = 96.91%). Conversely, R_p increased with increasing the concentration of the inhibitor. These results suggest that the addition of cerium nitrate inhibitor retards the oxygen reduction reaction. In agreement with previous investigations **[33-36]**, it is assumed here that reaction (1) triggered the formation of hydroxyl anions that further reacted with cerium cations [(2) and (3)] to result in CeO_2 as final product [(4) and (5)]:

$$O_2 + 2H_2O + 4e^- \rightarrow 4OH^- \qquad (1)$$

$$Ce^{3+} + 2OH^- \rightarrow Ce(OH)^+_2 \qquad (2)$$

$$Ce^{3+} + 3OH^- \rightarrow Ce(OH)_3 \downarrow \qquad (3)$$

In aerated solution, freshly precipitated $Ce(OH)_3$ is readily oxidized by oxygen forming tetravalent ceric hydroxide $Ce(OH)_4$ which further dehydrates to CeO_2 [**13-14**]:

$$4\ Ce(OH)_3 + O_2 + 2H_2O \rightarrow 4\ Ce(OH)_4 \qquad (4)$$

$$Ce(OH)_4 \rightarrow CeO_2 + 2\ H2O \qquad (5)$$

3.1.2. Electrochemical impedance behavior

The Nyquist and Bode plots of mild steel in 0.1M NaCl solution with and without various concentrations of cerium nitrate between 50 and 600 $mg.L^{-1}$ were recorded at the OCP after immersion samples for 30 minutes and are plotted in **Fig. 2** (**a & b**).

The EIS diagrams (Nyquist and Bode plots) of mild steel obtained without cerium nitrate inhibitor (blank) in NaCl solution after 30 minutes of immersion time showed the existence of two capacitive loops at HF (haut frequencies) and MF (middle frequencies) (**Fig 2. a & b**), that appeared to be a single capacitive loop. The first loop could be ascribed to the accumulation of corrosion products, and the second one in low frequency range was attributed to the charge transfer reaction. In addition, the phase of the Bode plot without inhibitor addition in NaCl solution was smaller than that with the presence of inhibitor, which reflects an increase in the corrosion rate on mild steel surface (**Fig. 2b)**. The same equivalent circuit was used by Marcelin *et al.* **[23]** to simulate the experimental data for the martensitic stainless steel in aerated and neutral medium where the impedance diagrams presented only one time constant but the experimental data were modelled using hierarchical parallel RC circuits. In the presence of the inhibitor, the general shape of Nyquist and Bode plots displayed a similar trend regardless of the concentration but the Nyquist size and impedance phase of the system gradually increased with increasing cerium nitrate concentration (**Fig. 2)**. In all cases, the diagrams exhibited a flattened capacitive loop, which was characterized by two uncoupled relaxation times, representing the film and charge transfer resistance at high and intermediate/low frequencies (HF and M-LF), respectively. According to Mishra *et al.* **[37]** the high frequency range gives information from the oxide film although the exact values can be affected by the structure, the defects and the composition of the layers while the intermediate and low frequencies correspond to the corrosion process at the electrochemical interface (metal/solution).

In essence, the impedance spectra did not show perfect semicircles typically associated with ideal capacitors. As such, the phase values (θ_{max}) are lower than (-90°) and the maximum phase angle did not exceed (-70°) in the Bode plots. Then, the responses of the impedance data without and with cerium nitrate inhibitor in 0.1M NaCl solution were modeled using simple electrical equivalent circuits presented in **Fig. 3**. According to Hamlaoui *et al.* **[20]**, R_s, R_c and R_{ct} are, respectively the solution resistance, the resistance of the outer porous layer, and the charge transfer resistance at the interface. Thus, the constant phase elements CPE_c and CPE_{dl} are the non-ideal (dispersive) layer capacitance, and double-layer capacitance, respectively. The presence of the double layer capacitance displayed dispersion effects by imperfections and

roughness of surface. Also, the n values falling within the range $0 \leq n \leq 1$ (n = 1 when CPE is pure capacitance) represent a non-linear coefficient, which varied with the electrode surface heterogeneity resulting from surface roughness. The results of the EIS data fitted with the Z_{view} software are presented in **Table 3 (**where χ^2 is the error factor**).** The data in **Table 3** show that the increasing additions of cerium nitrate to the NaCl solution allowed to increase the R_{ct} values and to reduce the CPE_{dl} ones in agreement with the d.c. polarization data of **Fig. 1b**. Overall, the electrochemical results demonstrated that the major corrosion inhibition was obtained with the addition of 600 mg/L of cerium nitrate. Therefore, the subsequent characterization was carried out only with this concentration of cerium nitrate.

The SEM images of mild steel obtained after 30 min of immersion in 0.1M NaCl solution are shown in **Figs. 4a** and **4b**. The surface was covered with corrosion products (dark contrast, **Fig. 4a**), which seem thick, heterogeneous and porous (**Fig. 4b**). Some parts of the surface remained unaffected (bright contrast, **Fig. 4a**). In contrast, the addition of 600 mg/L of cerium nitrate to the NaCl solution revealed a rather homogeneous film covering the whole of the surface of substrate after 30 min of immersion (**Fig. 4. c & d**). The film displayed a cracked (dry mud) morphology that was previously reported to arise from the shearing stresses between the film and the substrate upon drying of the film **[38]**. Also, the film contains some small-scattered nodules. The EDS analysis of the surface indicated that the films were rich in O (about 46 at%), in Fe (about 25 at%) and in Ce (11 at%) thus suggesting that the films were very thin. However and within EDS accuracy, there was no trace of Cl or of Na retained in the film. This can be explained by the rinsing of the samples after the test that removed both Na and Cl and/or because the chlorides could not permeate through the film. The latter were however reported to occur in cathodic electrodeposited ceria-based coatings whose microstructure was more open than the one obtained here by precipitation **[39]**. Furthermore, the presence of carbon (about 17 at%) suggests that a carbonated green rust could have formed as also demonstrated in previous studies with electrodeposited ceria coatings **[13]**.

The composition of rust formed on mild steel surface (blank) in 0.1M NaCl (without inhibitor) solution and after 30 min of immersion time is presented in **Fig. 5**. By considering the Raman shift values of previous studies for iron oxides **[40-42]**, the peaks at 224, 244, 290, 407,494, 608 and 1310 cm^{-1} correspond to hematite (α-Fe_2O_3), those at 377 and 1070 cm^{-1} are typical of

lepidocrocite (γ-FeOOH) while those at 345, 540 and 566 cm^{-1} correspond to magnetite (Fe_3O_4). The only peak at about 657 cm^{-1} could be related to maghemite (γ-Fe_2O_3) **[43-44]**.

In the presence of 600 $mg.L^{-1}$ of cerium nitrate in the 0.1M NaCl solution, there were far less peaks associated with the iron oxy-hydroxides. In contrast, the intense peak at about 459 cm^{-1} was attributed to the symmetric vibration of Ce-O of CeO_2 **[34, 45]**. The precise wavenumber and the shape of this peak can be strongly influenced by the particles size and the oxygen vacancies in the films **[34, 45-47]**. K. Aramaki showed that the presence of CeO_2 in the film, makes a more stable and protective coating in chloride media **[48]**. Also, a small particle size and minimum thickness of the film increase the corrosion resistance of the substrate **[49]**. The peaks at 433 and 511 cm^{-1} were attributed to Fe^{2+}-OH and Fe^{3+}-OH **[50]**. In addition, the occurrence of an intense peak at around 713 cm^{-1} typically ascribed to carbonates **[51-52]** confirms the adsorption of CO_2 from the air that leads to the formation of the carbonated green rusts **[13]**. These compounds could be identified through the small peak located at around 936 cm^{-1} that Hansen ascribed to [$Fe_2^{(II)}Fe_3^{(III)}(OH)_{12}CO_3, 2H_2O$] **[53]**. However, in the presence of chlorides, the stoichiometry $3Fe(OH)_2.Fe(OH)_2Cl.nH_2O$ with ($3 \geq n \geq 2$) was reported for green rusts **[54]**. Such green rusts are often stable upon the first stages of corrosion at pHs between 7 and 12, but are rapidly oxidized to lepidocrocite **[55]** or ferrihydrite **[56]**. Here, the Raman vibrations at 244, 290 and 1320 cm^{-1} and at 377 and 1086 cm^{-1} were respectively attributed to hematite (α-Fe_2O_3) and lepidocrocite (γ-FeOOH) but as opposed to the non-inhibited substrate, neither magnetite nor maghemite were detected.

In the presence of 600 $mg.L^{-1}$ of cerium nitrate inhibitor (with 0.1M NaCl), it thus likely that the weak acidity of the electrolyte (pH = 5.2) partly triggered corrosion of the substrate to result in Fe^{2+}, that in turn reacted with H_2O to develop iron hydroxide $Fe(OH)_2$, according to reaction (6).

$$Fe^{2+} + 2H_2O \rightarrow Fe(OH)_2 + 2H^+ + 2e^- \qquad (6)$$

The green rust (GR) then generated through reaction (7), involving Fe, $Fe(OH)_2$ and carbonate ion generated the CO_2 from the air.

$$Fe(OH)_2 + Fe^{2+} + CO_3^{2-} + 1/2\ O_2 + 3H_2O \rightarrow [Fe_2^{(II)}Fe_3^{(III)}(OH)_{12}][CO_3 2H_2O] \qquad (7)$$

Comparatively, the cerium nitrate inhibitor in NaCl media after 30 minutes of immersion time limited the generation of iron oxy-hydroxides but did not impede the formation of green rusts since CeO_2 is well-known to trap CO_2, hence to generate carbonates **[13]**.

3. 2. Effect of addition of PEG

Polyethylene glycol (PEG) has been extensively used in various sectors, such as biomedical, cosmetic and pharmacological applications **[57]**. In previous studies, PEG was for instance added to the electrolyte in order to create coatings having the capacity to increase corrosion resistance of Zn **[58]**. This present part is devoted to use the PEG as a corrosion inhibitor with cerium nitrate inhibitor (combined effect) in 0.1M NaCl media in order to increase both the corrosion resistance of the substrate and the stability of the obtained films. This choice is dictated by the consideration that PEG is a non-toxic inhibitor and respectful of the environment. Ashassi-Sorkhabi *et al.* **[59]** demonstrated that PEG in solution affects the physical properties of the medium by reducing both the pH and conductivity values of the NaCl solution (from pH = 5.2 and λ = 12. 21 $\mu S.cm^{-1}$ without PEG, to pH = 4.9 and λ = 10.57 $\mu S.cm^{-1}$ with PEG).

The effect of PEG addition (2.5 $g.L^{-1}$ with M = 15,000 g/mol; n = 33-34) in solution containing 0.1M NaCl and 600 $mg.L^{-1}$ cerium nitrate on the electrochemical response of the substrate after 30 minutes of immersion time and at room temperature was studied by using potentiodynamic and electrochemical impedance spectroscopy techniques (represented in **Fig. 6**). The results of potentiodynamic measurements and EIS data are represented in **Tables 4** and **5**, respectively. In the presence of PEG, the corrosion potential shifted (about 13 mV) towards less cathodic potentials compared to the one without PEG. In addition, a decrease of cathodic slope and a decrease of the anodic one was noticed when PEG was added. This allowed to reduce I_{corr} from 4.6 to 3.8 $\mu A/cm^2$ by adding PEG addition, which corresponds to an efficiency (IE) of about 97.5%. This indicates that PEG allowed to give more stability to the ceria-based layer, and to limit the anodic reaction of metal dissolution.

The Nyquist plots with and without PEG had the same shape (**Fig. 6b**), indicating that the electrochemical reaction taking place in the interface was not modified with the addition of PEG. From higher to low frequencies, the Nyquist diagrams showed the existence of two uncoupled relaxation times (coating and charge transfer resistance). Also, an increase of R_{ct} value was remarked with the presence of PEG. This is indicative of an inhibition effect of PEG on the surface of mild steel. In addition, the contradiction between the concomitant increase of both the R_{ct} and the CPE_{dl} with PEG addition can be related to a complex nature of the layer formed and to the partial breakdown of the surface film in some areas.

Fig. 7a shows the surface SEM before immersion. The above hypothesis on the discontinuity of the film is confirmed by the presence of two zones in the SEM image of **Fig. 7b** after 30 min of immersion in NaCl with 600 mg/L of cerium nitrate and addition of PEG. In the first zone, the surface morphology seemed relatively covered with worm-like features indicative of the adsorption/deposition of cerium derivatives on the PEG molecules adsorbed on the steel surface **[51]**. A small concentration of Ce (< 1 at%) was also detected by EDS. In contrast, the second zone was covered with a cerium-rich film (confirmed by EDS analysis). In spite of the two morphologically different zones, there was no sign of corrosion. It thus appears that the presence of the cerium-containing film and the adsorption of PEG to the steel surface following equation (8) hindered the formation of corrosion products **[18]**.

$$Fe^{3+} + HO(CH_2CH_2O)_n H \rightarrow H^+ + ([HO(CH_2CH_2O)_n]Fe^{3+}) \qquad (8)$$

According to the results obtained in this section, we conclude that the PEG addition allows to decrease the corrosion current density and increase corrosion resistance of mild steel in 0.1M NaCl solution after 30 minutes of immersion time. Thus, the presence of PEG reduces the numbers of nodules on surface mild steel. Moreover, the substrate dissolution reaction is inhibited.

3. 3. Effect of immersion time

In order to evaluate the corrosion current and the evolution of mild steel with and without inhibitor for long immersion times (30 days) in 0.1M NaCl, a series of tests was carried out by using potentiodynamic technique. The results are shown in **Fig. 8a**. Also, for comparative purposes, the polarization curves of mild steel immersed in a neutral 0.1M NaCl solution without (untreated) and with Ce and Ce + PEG for 30 days of immersion are shown in **Fig. 8b**. The corrosion potential shifted towards more electronegative values with PEG addition and with time (**Fig. 8a**) indicating that the corrosion rate in the aerated NaCl medium was under cathodic control (oxygen diffusion) in the presence of inhibitor. However, four stages could be identified in the untreated sample (**Table 6**). During the first stage (0-2 h), the potential quasi-stabilized due to the formation of the corrosion products film onto the surface. This brought about an increase of the current density (from ~149 to ~180 µA/cm^2). During the second stage (between 2 h and 1 day), the E_{corr} moved rapidly towards the cathodic domain, indicating the rapid degradation of the metal that led to a rapid increase of the current density (from ~180 to

~330. μA/cm^2). During the third stage (between 1 and 20 days), the current density (I_{corr}) decreased slowly, probably because the corrosion products formed on the surface physically blocked the oxidation reaction. Finally, during the fourth stage (between 20 and 30 days), there was a rapid decrease of the current density I_{corr} (from ~656 to ~427 μA/cm^2), and the potential corrosion (E_{corr}) moved to anodic domains (from -603 to -503 mV/SCE). This can be due to the development of the barrier (passive) film of corrosion product on the substrate.

When the solution contains Ce or Ce+PEG, the E_{corr} was lower than in the blank solution already after 30 min, which is indicative of the formation of Ce oxi-hydroxide film on the surface **[34]**. However, the E_{corr} was stabilized in the presence of PEG but not in its absence (**Table 6**). It thus appears that the beneficial effect of Ce was superseded by the growth of corrosion products. Conversely, the values of the current densities with time were much lower in the presence of Ce than in the blank solution, in particular when PEG was also added (**Table 6**).

For illustration purposes, **Fig. 8b** gathers the polarization curves of mild steel after immersion in 0.1M NaCl for 30 days. Clearly, the addition of PEG to the cerium nitrate containing solutions drastically inhibited the corrosion and allowed to maintain the stability of the Ce oxi-hydroxide film after 30 days of immersion. According to the calculated values in **Table 6**, it is observed that the efficiency of the corrosion inhibitor (IE) remains almost stable during the whole immersion period reaching a value close to ~97% against just ~85% in the absence of PEG.

The impedance diagrams (**Fig. 9a & b**) of mild steel were carried out in 0.1M NaCl solution as function of immersion time up to 30 days. An equivalent circuit similar to the one inserted in **Fig. 9a** is proposed for modeling the impedance data (**Table 7**). Between 30 min and 8 hours, the equivalent circuit proposed is that of **Fig. 3**. After 1 day of immersion time of mild steel in 0.1M NaCl media, a resistance (W) related to the appearance of a diffusion resistance had to be added to the equivalent circuit. According to the literature, the immersion of mild steel in NaCl solution results in a diffusion resistance that suggests the diffusion of oxygen and reactive species at the interface between the solution and the surface **[60]**, where W_{1R}, W_{1T} and W_{1P} are the diffusion resistance, diffusion capacitive and diffusion of non-linear coefficient, respectively. The data of **Table 7** clearly indicates that there was a decrease of the transfer resistance and an increase of the CPE_{dl} values with increasing of immersion time. This denotes

the continued degradation of the surface and that the rust layers grew in thickness with immersion time as also observed in **[61]**. Between 20 and 30 days, it could noticed that the transfer resistance increased, which is probably due to the formation of a passive film that protected the surface of the substrate. **Figures 9 (c)** to **(f)** show the EIS (Nyquist and Bode) diagrams with and without PEG addition (an equivalent circuit is proposed in **figure 9c** and **e**, for modeling the impedance data-**Table 7**). The spectra consisted of two uncoupled relaxation times, that represent the film and charge transfer resistance at high and intermediate/low frequencies (HF and M-LF), respectively. If cerium is added to the solution, a continuous decrease of the R_{ct} values is observed and then remain constant for the longest immersions. The R_{ct} values for the solution with cerium are about 2000 Ω.cm². With the addition of PEG, the R_{ct} values started to decrease after a short period of immersion, indicating that the film formed at the surface allowed the penetration of water and of aggressive ions. Still, the R_{ct} values remained higher (R_{ct} = 5350 Ω cm^2 than without the addition of PEG. The increase of the capacitance of the double layer with immersion times in both cases (more evident in the case of Ce+PEG) may result from the relatively higher dielectric constant of the defective coating upon water uptake **[62]**. Indeed, the electroless thin layers formed on carbon steel have been shown to contain also defects (see SEM surface images of Figs. 4c and 4d). This implies that the metal is not fully covered**.**

Fig. 10 gathers the morphology of the different surfaces (bare, cerium-modified and Ce+PEG modified) after 30 days of immersion in 0.1M NaCl. The surface of the bare steel surface was totally covered with corrosion products indicating the advanced degradation of this surface (**Fig. 10a**). At higher magnifications (**Fig. 10b**), needle-like crystals composed the nodules at the surface. In the presence of Ce, the surface was covered with a thin cracked layer (**Fig. 10c**) over which different corrosion nodules grew (**Fig. 10d**). In contrast, most of the surface was covered with an even film (**Fig. 10e**) and had a very fine microstructure that contained less cracks and less nodules (**Fig. 10f**) when Ce+PEG was added to the NaCl solution. The film was mainly composed of Ce, O and C according to the EDS analysis of **Fig. 10g**. However, such film was supposed to be very thin since the main elements of the substrate were also detected. Chlorine was also detected in low amounts on the surface.

In order to identify the corrosion products onto mild steel surface as function of immersion time from 1 to 30 days in 0.1M NaCl solution with Ce+PEG addition, the rusts layer were analyzed by using Raman spectroscopy presented in **Fig. 11**. The vibrations at around (244 cm^{-1}), (309,

1079 and 1130 cm^{-1}), (351, 1190 and 1370 cm^{-1}), (377 and 530 cm^{-1}), (673 cm^{-1}) and (730 cm^{-1}) are, respectively, indicative of hematite (α-Fe_2O_3), goethite (α-FeOOH), maghemite (γ-Fe_2O_3), lepidocrocite (γ-FeOOH), magnetite (Fe_3O_4) and akaganeite (β-FeOOH). They appeared from the first day of immersion in the solution and remained almost stable until the end of immersion (30 days) **[34, 63]**. Akaganeite disappeared after 30 days and the final corrosion products left were hematite, goethite, maghemite, lepidocrocite and magnetite. Additional vibrations of iron hydroxychloride (β-$Fe_2(OH)_3Cl$) at around (423 and 618 cm^{-1}) **[64]** appeared after 10 days of immersion. This compound was also detected in films after 30 days of immersion. This is very much in agreement with the EDS analysis of **Fig. 10g** that revealed Cl on the surface.

In addition, the symmetric vibration of Ce-O of CeO_2 appeared at about 456 cm^{-1} **[21]**. The position of Ce-O band shifted with increasing the immersion time: 456 cm^{-1} (1-3 days), 452 cm^{-1} (10 days) and 446 cm^{-1} (30 days) and was attributed to the evolution of particle size and of the oxygen vacancies in the film **[13]**.

The X-ray pattern of the film obtained with Ce+PEG is given in **Fig. 12**. The peaks appeared shadowed by a hump at low diffraction angles typical of amorphous compounds. Nevertheless, the characteristic peak of CeO_2 at about 47° and of Ce(III) oxy-hydroxide at about 27° were observed, as also reported in literature **[13, 72]**. Moreover, some peaks associated with γ-Fe_2O_3, α-FeOOH, Fe_3O_4 and α-Fe_2O_3 **[65]** were also identified. The appearance of peak at 10.6° could be attributed to the carbonate green rust GR(CO_3^{2-}) (**reaction 7**) similar to the ones reported by Hamlaoui *et al.* **[13]**.

The comparison of the films obtained after 30 days of immersion in 0.1M NaCl solution with and without PEG addition was investigated by Raman spectroscopy and the results are given in **Fig. 13** and **Table 8**). The composition of the main corrosion products formed on mild steel surface after 30 days of immersion time in chloride media without PEG addition are essentially composed of hematite, goethite, maghemite, lepidocrocite, magnetite and akaganeite. However, no peak of CeO_2 was detected. On the other hand, with PEG addition, akaganeite could not be observed in the spectra after 30 days of immersion time. In this case, it has been suggested that OH^- and Cl^- react concurrently with Fe^{3+} to produce lepidocrocite but not akaganeite **[66]**. Moreover, a small hump of CeO_2 was observed at around 446 cm^{-1}, suggesting that the PEG maintains the stability of this film after one month of immersion.

4. Conclusions

The corrosion inhibition of mild steel with the addition of cerium nitrate and of a combination of cerium nitrate and PEG was studied in 0.1M NaCl solutions. We have demonstrated that cerium nitrate acted as a cathodic inhibitor at least for 30 min of immersion time. The effect is more clearly marked with increasing the concentration to 600 $mg.L^{-1}$. The inhibition effect was procured by a film formed at the surface that contained CeO_2. However, inhibition was lost with increasing immersion time to such extent that no cerium-derivatives could be identified.

In contrast, the addition of 2.5 $g.L^{-1}$ of PEG to the cerium nitrate containing 0.1M NaCl solution increased further the corrosion inhibition through the formation of a thin and barely cracked film at the surface of the steel for the short times. After prolonged immersion in 0.1M NaCl for 30 days, the corrosion inhibition began to be lost through the formation of hematite, goethite, lepidocrocite, maghemite and magnetite and some green rusts. However, the attack was much reduced compared to the PEG-free surfaces since traces of CeO_2 and $Ce(OH)_3$ were still detected at the surface of the steel after 30 days of immersion.

References

[1] R. C. Zeng, W. Dietzel, W. J. Huang, K. U. Kainer, R. Zettler, J. Zhang, Review of studies on corrosion of magnesium alloys, Trans. Nonferrous Met. Soc. China. 16 (2006) s763-s771.

[2] F. Atmani, D. Lahem, M. Poelman, C. Buess-Herman, M.-G. Olivier, Mild steel corrosion in chloride environment: effect of surface preparation and influence of inorganic inhibitors, J. Corros. Eng. Sci. Techn. 48 (2013) 9-18.

[3] A. C. Bastos, M. G. Ferreira, and A. M. Simoes, Corrosion Inhibition by Chromate and Phosphate Extracts for Iron Substrates Studied by EIS and SVET, Corros. Sci. 48 (2006) 1500-1512.

[4] D. G. Shchukin, M. Zheludkevich, K. Yasakau, S. Lamaka, M. G. S. Ferreira, H. Möhwald, Layer-by-layer assembled nanocontainers for self-healing corrosion protection, Adv. Mater. 18 (2006) 1672-1678.

[5] M. Costa, C. B. Klein, Toxicity and carcinogenicity of chromium compounds in humans, Crit. Rev. Toxicol. 36 (2006) 63-155.

[6] M. A. Arenas, J. de Damborenea, Interference by cerium cations during the multi-step zinc dissolution process in a chloride-containing electrolyte, Corros. Sci. 48 (2006) 3196-3207.

[7] W. Liu, F. Cao, A. Chen, L. Chang, J. Zhang, Ch. Cao, Corrosion behaviour of AM60 magnesium alloys containing Ce or La under thin electrolyte layers. Part 1: Microstructural characterization and electrochemical behavior, Corros. Sci. 52 (2010) 627-638.
[8] M. Machkova, E. A. Matter, S. Kozhukharov, V. Kozhukharov, Effect of the anionic part of various Ce(III) salts on the corrosion inhibition efficiency of AA2024 aluminium alloy, Corros. Sci. 69 (2013) 396-405.
[9] J. Liu, D. Wang, L. Gao, D. Zhang, Synergism between cerium nitrate and sodium dodecylbenzenesulfonate on corrosion of AA5052 aluminium alloy in3 wt.% NaCl solution, Appl. Surf. Sci. 389 (2016) 369-377.
[10] B. R. W. Hinton, L. Wilson, The corrosion inhibition of zinc with cerous chloride, Corros. Sci. 29 (1989) 967-985.
[11] M. Bethencourt, F. J. Botana, J. J. Calvino, M. Marcos, M. A. Rodríguez-Chacón, Lanthanide compounds as environmentally-friendly corrosion inhibitors of aluminium alloys: a review, Corros. Sci. 40 (1998) 1803-1819.
[12] M. Bahmaeia, R. Pourzarea, A. Ghezloo, The effect of cerium pre-treatment on the corrosion resistance of steel sheets, Russ. J. Gen. Chem. 83 (2013) 2386-2391.
[13] Y. Hamlaoui, L. Tifouti, F. Pedraza, Investigation of electrodeposition cerium oxide based films on carbon steel and of the induced formation of carbonated green rusts, Corros. Sci. 50 (2008) 2182-2188.
[14] F. El-Taib Heakal, O. S. Shehata, N. S. Tantawy, Enhanced corrosion resistance of magnesium alloy AM60 by cerium (III) in chloride solution, Corros. Sci. 56 (2012) 86-95.
[15] E. Onofre-Bustamante, M. A. Domínguez-Crespo, A. M. Torres-Huerta, A. Olvera-Martínez, J. Genescá-Llongueras, F. J. Rodríguez-Gómez, Characterization of cerium-based conversion coatings for corrosion protection of AISI-1010 commercial carbon steel, J. Solid. State. Electrochem. 13 (2009) 1785-1799.
[16] H. Ashassi-Sorkhabi, N. Ghalebsaz-Jeddi, Inhibition effect of Polyethylene Glycol on the corrosion of carbon steel in sulphuric acid, Mater. Chem. Phy. 92 (2005) 480-486.
[17] H. Ashassi-Sorkhadi, N. Ghalebsaz-Jeddi, F. Hashemzadeh, H. Jahani, Corrosion inhibition of carbon steel in Hydrochloric acid by some Polyethylene Glycols, Electrochim. Acta. 51 (2006) 3848-3854.
[18] E. Guilminot, F. Dalard, C. Degrigny, Mechanism of iron corrosion in water-polyethylene glycol (PEG 400) mixtures, Corros. Sci. 44 (2002) 2199-2208.

[19] S. Salimi, M. Nasr-Esfahani, S. A. Umoren, E. Saebnoori, Complexes of imidazole with Poly (ethylene glycol) as a corrosion inhibitor for carbon steel in sulphuric acid, J. Mater. Eng. Perform. 24 (2015) 4696-4709.
[20] Y. Hamlaoui, L. Tifouti, F. Pedraza, Corrosion protection of electro-galvanized steel by ceria-based coatings: Effect of polyethylene glycol (PEG) addition, J. Mater. Eng. Perform. 22 (2013) 2706-2715.
[21] Y. Hamlaoui, H. Boudellioua, L. Tifouti, F. Pedraza, Corrosion resistance of electro-galvanized steel coated with PEG-modified ceria layers in chloride and sulfate media, J. Mater. Eng. Perform. 24 (2015) 4626-4635.
[22] L. G. Ecco, S. Rossi, F. Deflorian, M. Fedel, Colloidal cerium oxide nanoparticules: Preparation and corrosion inhibition performance on AA5005 aluminum alloy, J. Electrochem. Soc. 165 (2013) C88-C93.
[23] S. Marcelin, N. Pébère, S. Régnier, Electrochemical characterisation of a martensitic stainless steel in a neutral chloride solution, Electrochim. Acta. 87 (2013) 32-40.
[24] F. Arjmand, A. Adriaens, Influence of pH and chloride concentration on the corrosion behavior of unalloyed copper in NaCl Solution: A comparative study between the micro and macro scales, Materials. 5 (2012) 2439-2464.
[25] H. Boudellioua, Y. Hamlaoui, L. Tifouti, and F. Pedraza, Comparison between the inhibition efficiencies of two modification processes with PEG–ceria based layers against corrosion of mild steel in chloride and sulfate media, J. Mater. Eng. Perform. 26 (2017) 4402-4414.
[26] H. Shi, E. H. Han, F. Liu, Corrosion protection of aluminium alloy 2024-T3 in 0.05 M NaCl by cerium cinnamate, Corros. Sci. 53 (2001) 2374-2384.
[27] K. Aramaki, Self-healing protective film prepared on zinc electrodes by treatment in a cerium (III) nitrates solution and modification with sodium phosphate and calcium or magnesium nitrate, Corros. Sci. 45 (2003) 2361-2376.
[28] M. Hosseini, H. Ashassi-Sorkhabi, H. A. Yaghobkhani Ghiasvand, Corrosion protection of electro-galvanized steel by green conversion coatings, J. Rare. Earth. 25 (2007) 537-543.
[29] B. R. W. Hinton, Corrosion inhibition with rare earth metal, J. Alloy. Compd. 180 (1992) 15-25.
[30] A. J. Davenport, H. S. Issacs, M. W. Kendig, Corros. Sci. 32 (1991) 653-663.
[31] M. R. Majdi, I. Danaee, S. S. Seyyed Afghahi, Preparation and Anti-Corrosive Properties of Cerium Oxide Conversion Coatings on Steel X52, Materials Research. 20 (2017) 445-451.

[32] M. Stern, A. L. Geary, Electrochemical Polarization I. A Theoretical Analysis of the Shape of Polarization Curves, J. Electrochem. Soc. 104 (1957) 56-63.
[33] B. R. W. Hinton, D. R. Arnott, N. E. Ryan, The inhibition of aluminium alloy corrosion by cerous cation, Met. Forum. 7 (1984) 211-217.
[34] Y. Hamlaoui, F. Pedraza, C. Remazeilles, S. Cohendoz, C. Rébéré, L. Tifouti, J. Creus, Cathodic electrodeposition of Cerium-based oxides on carbon steel from concentrated cerium nitrate solutions. Part I. Electrochemical and analytical characterization, Mater. Chem. Phys. 113 (2009) 650-657.
[35] L. Martínez, E. Román, J. L. de Segovia, S. Poupard, J. Creus, F. Pedraza, Surface study of cerium oxide based coatings obtained by cathodic electrodeposition on zinc, Appl. Surf. Sci. 257 (2011) 6202-6207.
[36] B. Bouchaud, J. Balmain, G. Bonnet, F. Pedraza, pH-distribution of cerium species in aqueous systems, J. Rare. Earth. 30 (2012) 559-562.
[37] A. K. Mishra, R. Balasubramaniam, Corrosion inhibition of aluminium by rare earth chlorides, Mater. Chem. Phys. 103 (2007) 385-393.
[38] B. Bouchaud, J. Balmain, G. Bonnet, F. Pedraza, Optimizing structural and compositional properties of electrodeposited ceria coatings for enhanced oxidation resistance of a nickel-based superalloy, Appl. Surf. Sci. 268 (2013) 218-224.
[39] S. Poupard, F. Pedraza, J. Creus, Diffusion of a corroding electrolyte through defective electroplated ceria based coatings, Defect & Diffusion Forum 289-292 (2009) 235-242.
[40] D. C. Smith, A. Barbet, A preliminary Raman microscopic exploration of pigments in wall paintings in the roman tomb discovered at Kerch, Ukraine, in 1891, J. Raman. Spectrosc. 30 (1999) 319-324.
[41] D. de la Fuente, J. Alcántara, B. Chico, I. Díaz, J. A. Jiménez, M. Morcillo, Characterisation of rust surfaces formed on mild steel exposed to marine atmospheres using XRD and SEM/Micro-Raman techniques, Corros. Sci. 110 (2016) 253-264.
[42] X. Zhang, K. Xiao, C. Dong, J. Wu, X. Li, Y. Huang, In situ Raman spectroscopy study of corrosion products on the surface of carbon steel in solution containing Cl^- and SO_4^{2-}, Eng. Fail. Anal. 18 (2011) 1981-1989.
[43] J. K. Singh, D. D. N. Singh, The nature of rusts and corrosion characteristics of low alloy and plain carbon steel in three kinds of concrete pore solution with salinity and different pH, Corros. Sci. 56 (2012) 129-142.

[44] W. Chen, R-G. Du, Ch-Q. Ye, Y-F. Zhu, Ch-J. Lin, Study on the corrosion behavior of reinforcing steel in simulated concrete pore solutions using in situ Raman spectroscopy assisted by electrochemical techniques, Electrochim. Acta. 55 (2010) 5677-5682.

[45] J. Creus, F. Brezault, C. Rebere, M. Gadouleau, Synthesis and characterization of thin cerium oxide coatings elaborated by cathodic electrolytic deposition on steel substrate, Surf. Coat. Tech. 200 (2006) 4636-4645.

[46] A. Siokou, S. Ntais, V. Dracopoulos, S. Papaefthimiou, G. Leftheriotis, P. Yianoulis, Substrate related structural, electronic and electrochemical properties of evaporated CeOx ion storage layers, Thin Solid Films. 514 (2006) 87-96.

[47] F. Pedraza, J. Balmain, G. Bonnet, B. Bouchaud, Novel concept of functional oxide coatings providing enhanced oxidation resistance to Ni-based superalloys, Mater. Res. Bull. 49 (2014) 384-387.

[48] K. Aramaki, The effect of modification with hydrogen peroxide on a hydrated cerium(III) oxide layer for protection of zinc against corrosion in 0.5 M NaCl, Corros. Sci. 48 (2006) 766-782.

[49] M. F. Montemor, A. M. Simoes, M. G. S. Ferreira, Composition and corrosion behavior of galvanized steel treated with rare-earth salts: the effect of the cation, Prog. Org. Coat. 44 (2002) 111-120.

[50] H. Kanno, Hydrations of metal ions in aqueous electrolyte solutions: a Raman study, J. Phys. Chem. 92 (1988) 4232-4236.

[51] Y. Hamlaoui, L. Tifouti, C. Remazeilles, F. Pedraza, Cathodic electrodeposition of cerium based oxides on carbon steel from concentrated cerium nitrate. Part II: Influence of electrodeposition parameters and of the addition of PEG, Mater. Chem. Phys. 120 (2010) 172-180.

[52] M. Villanueva-Ibanez, C. Le Luyer, S. Parola, C. Dujadin, J. Mugnier, Influence of Sr/Hf ration and annealing treatment on structural and scintillating proprieties of Sol-gel Ce^{3+} doped strontium hafnate powders, Opt. Mater. 27 (2005) 1541-1546.

[53] H. C. B. Hansen, Access Denied Composition, stabilization, and light absorption of Fe(II)Fe(III) hydroxy-carbonate (green rust), Clay. Miner. 24 (1989) 663-669.

[54] L. Legrand, G. Sagon, S. Lecomte, A. Chausse, R. Messina, A Raman and infrared study of a new carbonate green rust obtained by electrochemical way, Corros. Sci. 43 (2001) 1739-1749.

[55] T. Misawa, K. Hashimoto, S. Shimodaria, The mechanism of formation of iron oxide and oxyhydroxides in aqueous solutions at room temperature, Corros. Sci. 14 (1974) 131-149.

[56] A. Manceau, W. P. Gates, Surface structural model for ferrihydrite, Clay. Clay. Miner. 45 (1997) 448-460.
[57] M. J. Harris, S. Zalipsky, Poly (ethylene glycol) Chemistry and Biological Applications, American Chemical Society, Washington, 1997, Chapter 1, p1-13.
[58] J. Dobryszycki, S. Biallozor, On some organic inhibitors of zinc corrosion in alkaline media, Corros. Sci. 43 (2001) 1309-1319.
[59] H. Ashassi-Sorkhabi, S. A. Nabavi-Amri, Polarization and impedance methods in corrosion inhibition study of carbon steel by amines in petroleum–water mixtures, Electrochim. Acta. 47 (2002) 2239-2244.
[60] C. N. Cao, J. Q. Zhang, An introduction to electrochemical impedance, Beijing, Science Press, 2002.
[61] Y. Ma, Y. Li, F. Wang, Corrosion of low steel in atmospheric environments of different chloride content, Corros. Sci. 51 (2009) 997-1006.
[62] C. Wang, F. Jiang, F. Wang, The characterization and corrosion resistance of cerium chemical conversion coatings for 304 stainless steel, Corros. Sci. 46 (2004) 75-89.
[63] D. L. A. de Faria, S. V. Silva, M. T. de Oliveira, Raman microspectroscopy of some iron oxides and oxyhydroxides, J. Raman. Spectrosc. 28 (1997) 873-878.
[64] S. Réguer, D. Neff, L. Bellot-Gurlet, P. Dillmann, Deterioration of iron archaeological artefacts: micro-Raman investigation on Cl^- containing corrosion product, J. Raman. Spectrosc. 38 (2007) 389-397.
[65] JCPDS. International Centre for diffraction Data, Edition 2011.
[66] K. Xiao, C. F. Dong, X. LI, Corrosion products and formation of mechanism during initial stage of atmospheric corrosion of carbon steel, J. Iron. Steel. Res. Int. 15 (2008) 42-48.
[67] T. Ohtsuka, Raman Spectra of passive films of iron in neutral borate solution, Mater. T. Jim. 37 (1996) 67-69.
[68] R. J. Thibeau, R. J. Brown, R. H. Heidersbach, Raman spectra of possible corrosion products of iron, Appl. Spectrosc. 32 (1978) 532-535.
[69] B. Yashwansingh, R. Surnam, Cheng-Wei Chui, Huaping Xiao, Hong Liang, Investigating atmospheric corrosion behavior of carbon steel in coastal regions of Mauritius using Raman Spectroscopy, Rev. Mater. 12 (2016) 157-168.
[70] R. Balasabramaniam, A. V. Rameshkamar, P. Dillmann, Characterization of rust on ancient Indian iron, Corr. Sci. India. 85 (2003) 1546-1555.

[71] L. Slavov, M. V. Abrashev, T. Merodiiska, Ch. Gelev, R. E. Vandenberghe, I. Markova-Deneva, I. Nedkov, Raman spectroscopy investigation of magnetite nanoparticles in ferrofluids, J. Magn. Magn. Mater. 322 (2010) 1904-1911.
[72] V. Lair, J. Sirieix-Plenet, L. Gaillon, C. Rizzi, A. Ringuedé, Mixtures of room temperature ionic liquid/ethanol solutions as electrolytic media for cerium oxide thin layer electrodeposition, Electrochim. Acta 56 (2010) 784-789.

Figure 1: (a) OCP evolution with immersion time (b) Potentiodynamic polarization curves for mild steel in 0.1M NaCl solution at room temperature with increase concentration of cerium nitrate inhibitor.

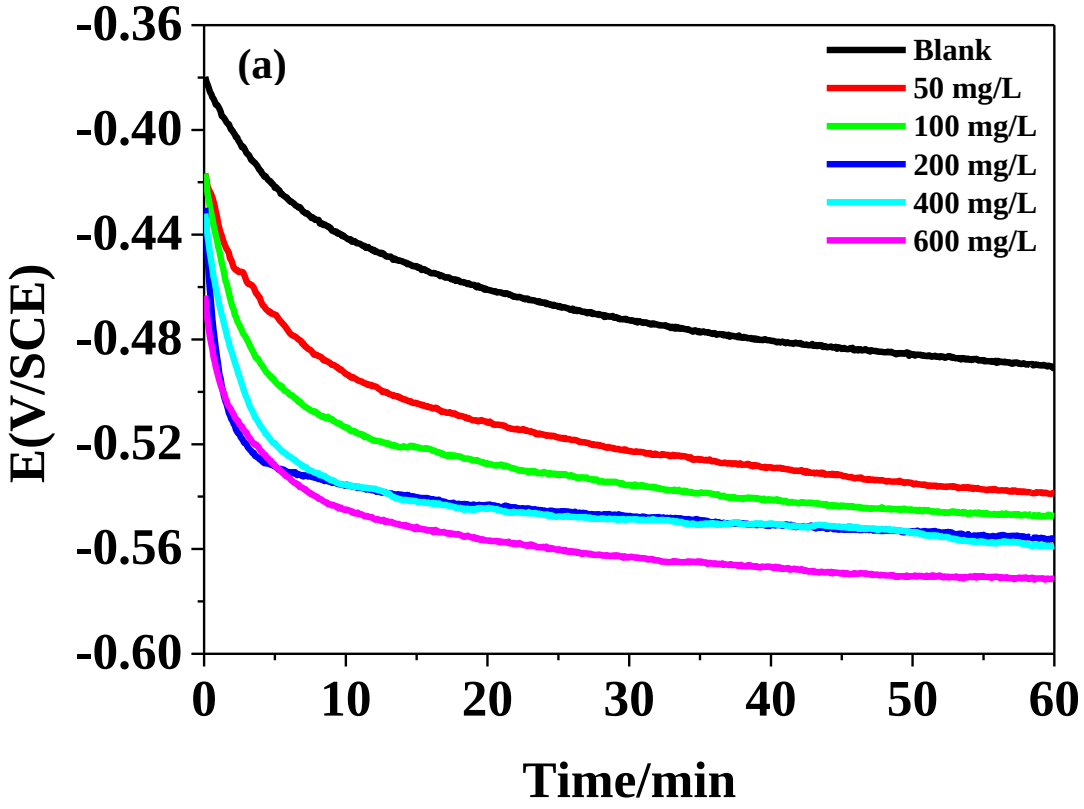

Figure 1a

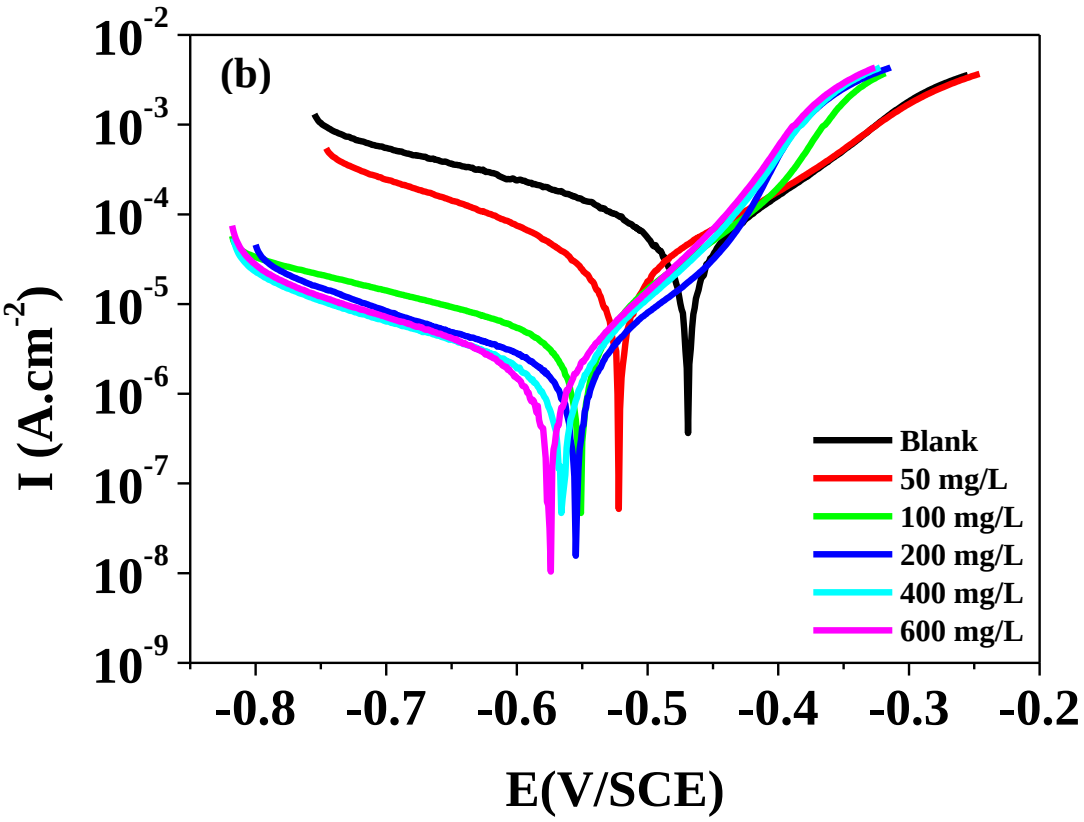

Figure 1b

Figure 2: Electrochemical impedance spectra of (a) Nyquist and (b) Bode plots for mild steel in 0.1M NaCl solution as a function of various concentrations of cerium nitrate after 30 minutes exposure at room temperature.

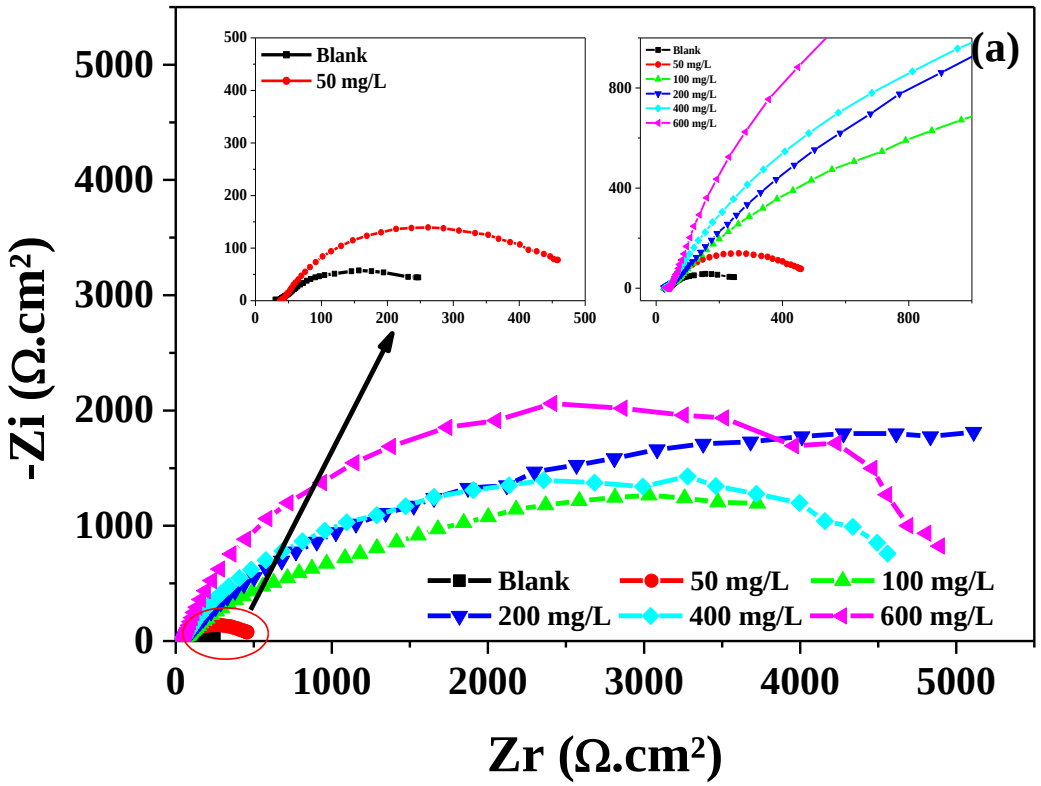

Figure 2a

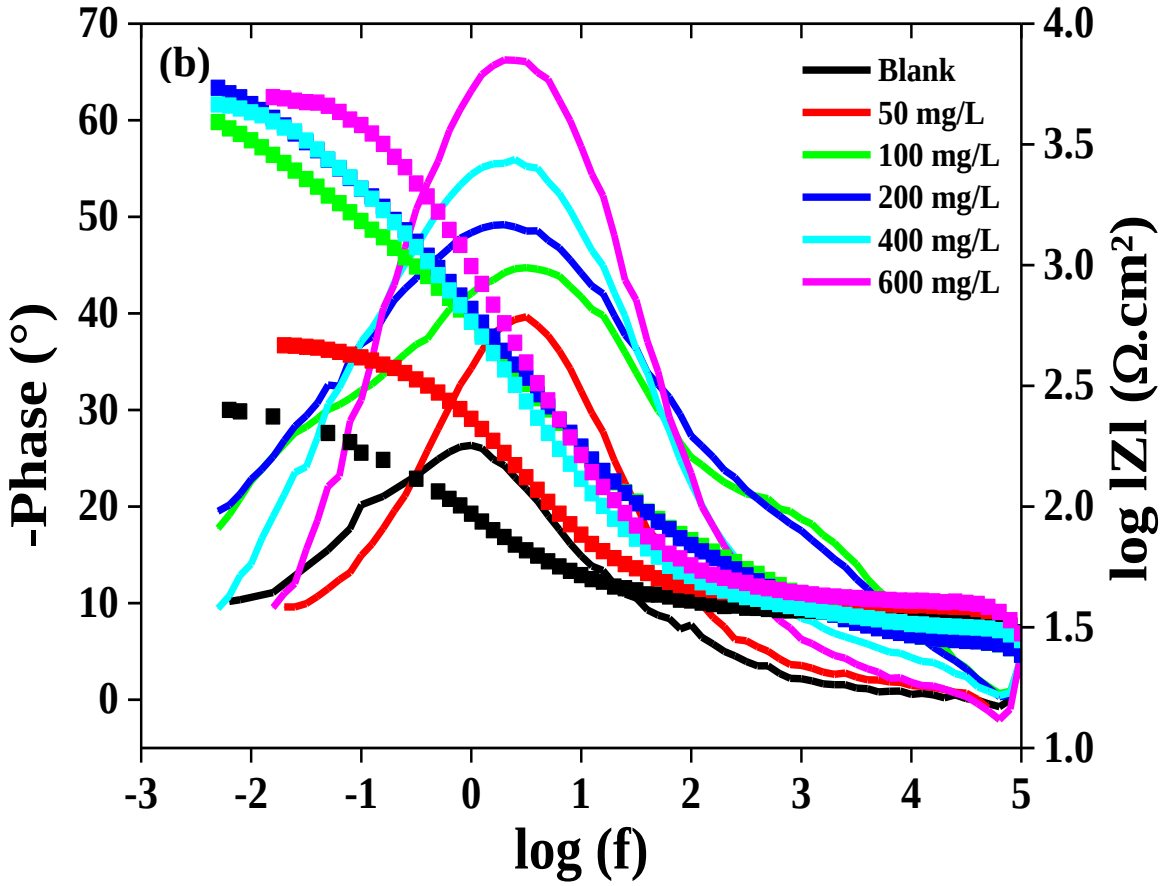
(b)
Blank
50 mg/L
100 mg/L
200 mg/L
400 mg/L
600 mg/L
-Phase (°)
log |Z| (Ω.cm²)
log (f)
70
60
50
40
30
20
10
0
4.0
3.5
3.0
2.5
2.0
1.5
1.0
-3
-2
-1
0
1
2
3
4
5

Figure 2b

Figure 3: Electrical equivalent circuit used for samples without and with various concentrations of cerium nitrate after immersion in 0.1M NaCl solution for 30 minutes.

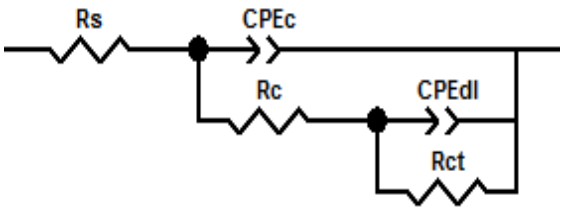

Figure 4: SEM images of ASTM A915 mild steel: (a) surface appearance after 30 min in 0.1M NaCl, (b) is a zoomed image of (a). (c) is the same condition in the presence of 600 $mg.L^{-1}$ of cerium nitrate and (d) a zoomed image of selected part. (e) is the corresponding EDS spectrum.

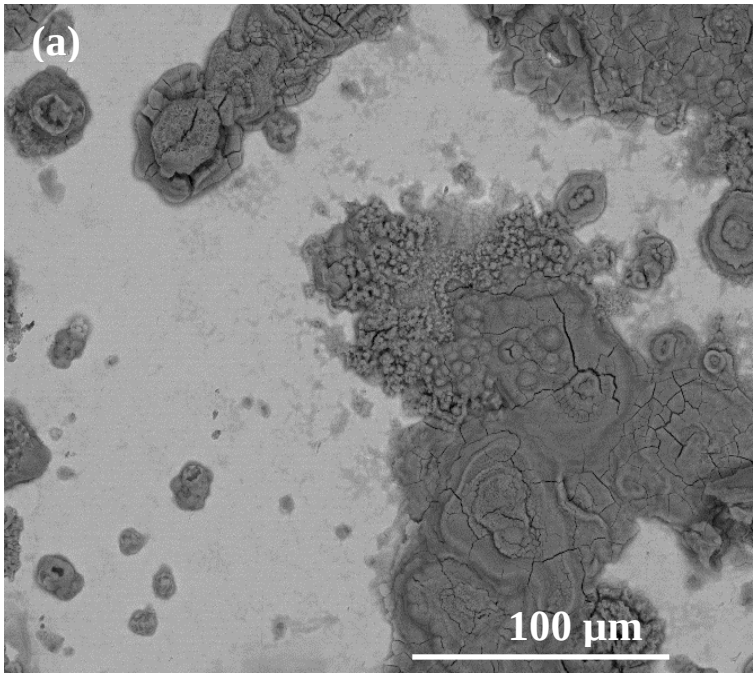

Figure 4a

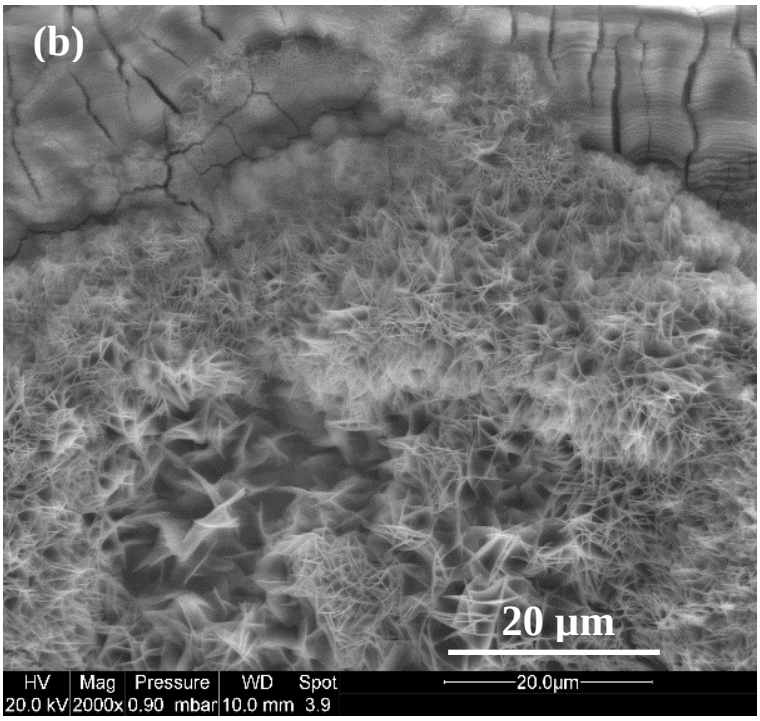
(b)
20 µm
HV Mag Pressure WD Spot
20.0 kV 2000x 0.90 mbar 10.0 mm 3.9
20.0µm

Figure 4b

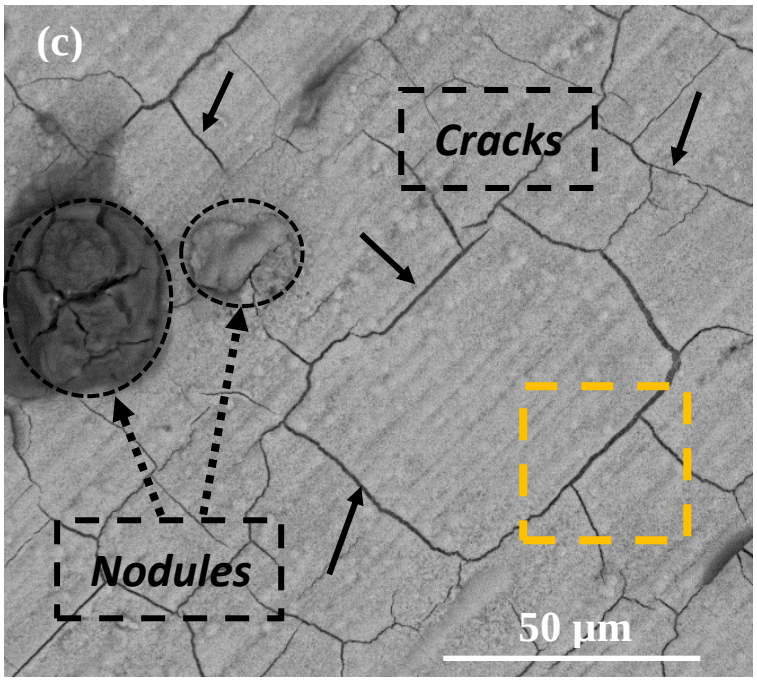

Figure 4c

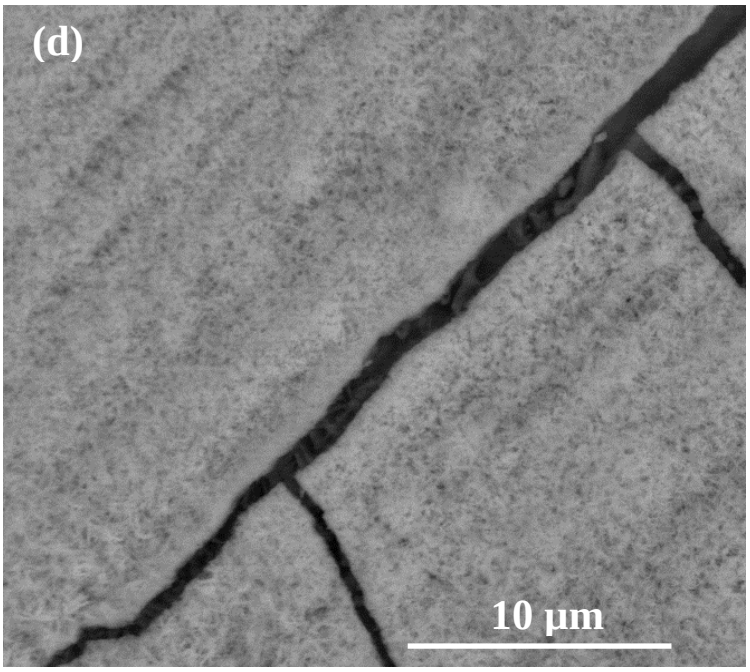

Figure 4d

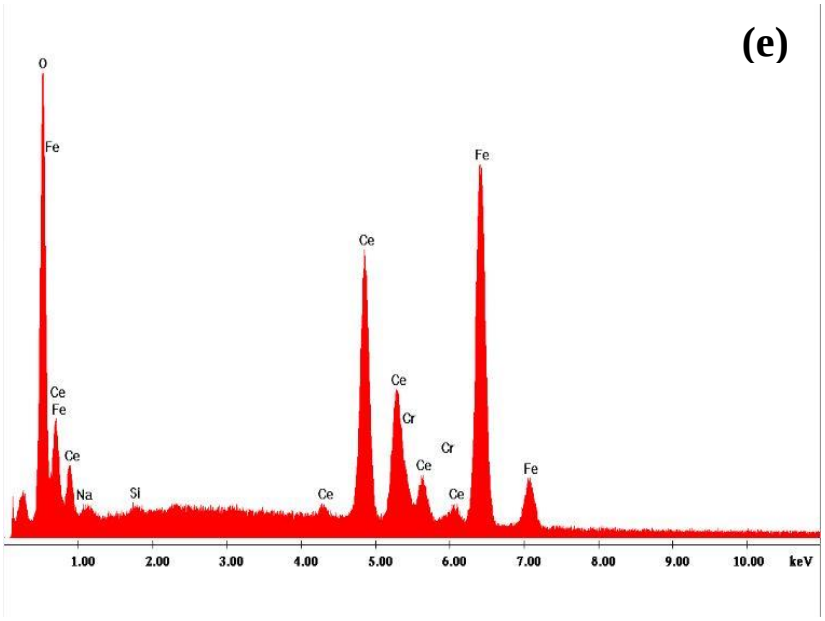
(e)
O
Fe
Ce
Fe
Ce
Na
Si
Ce
Ce
Fe
Ce
Cr
Cr
Ce
Ce
Fe
1.00
2.00
3.00
4.00
5.00
6.00
7.00
8.00
9.00
10.00
keV

Figure 4e

Figure 5: Raman spectra of mild steel samples without and with 600 mg.L^{-1} of cerium nitrate in 0.1M NaCl solution after 30 min of immersion time, at room temperature.

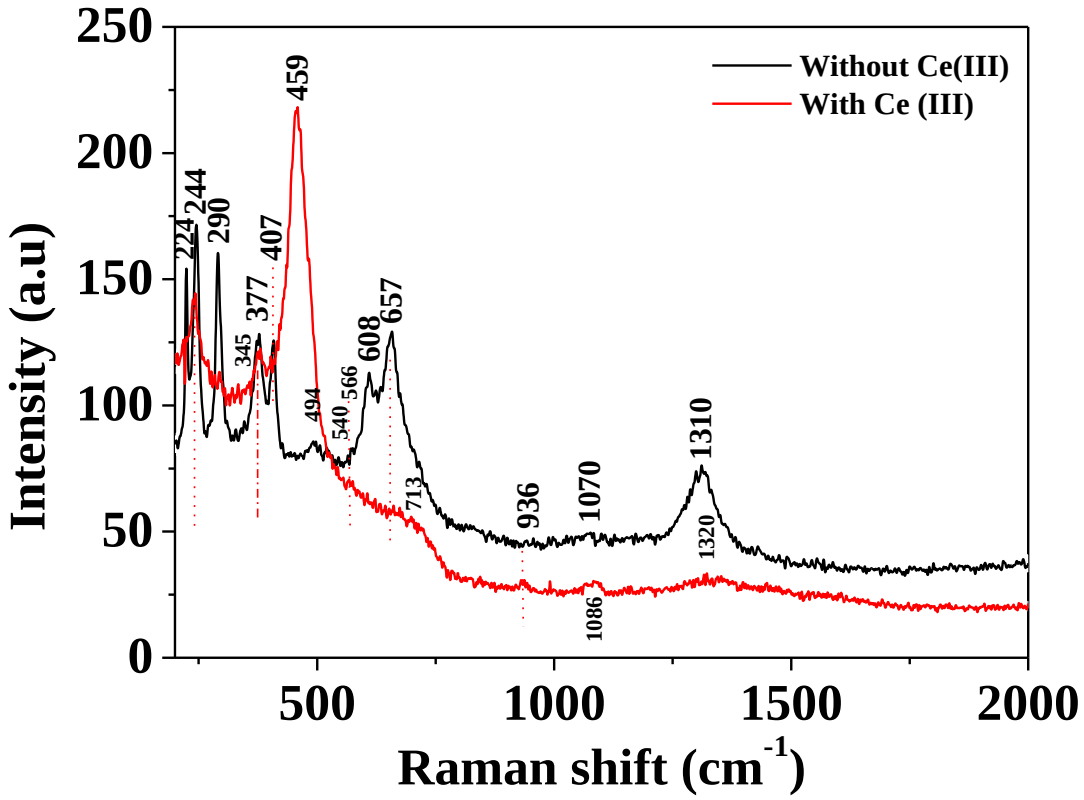

Figure 6: Potentiodynamic polarization curves (a) and EIS diagrams (Nyquist) (b) for mild steel recorded in 0.1M NaCl solution with and without PEG addition for 30 min of immersion time.

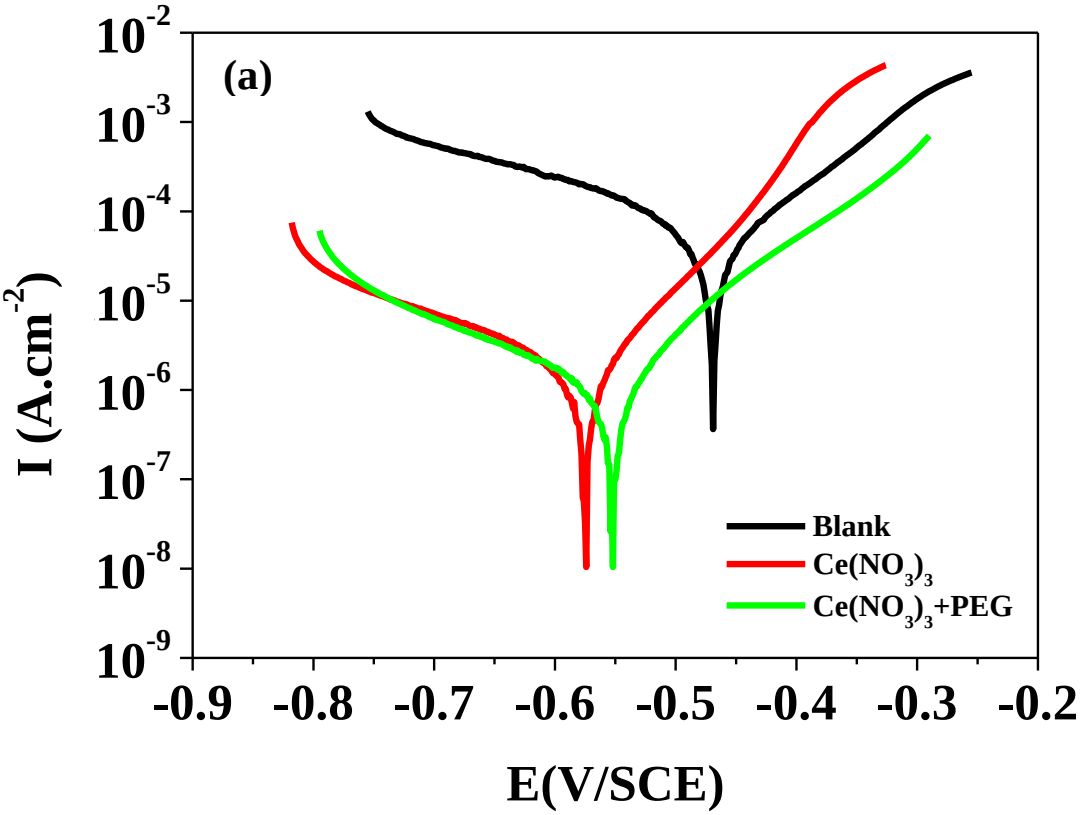

Figure 6a

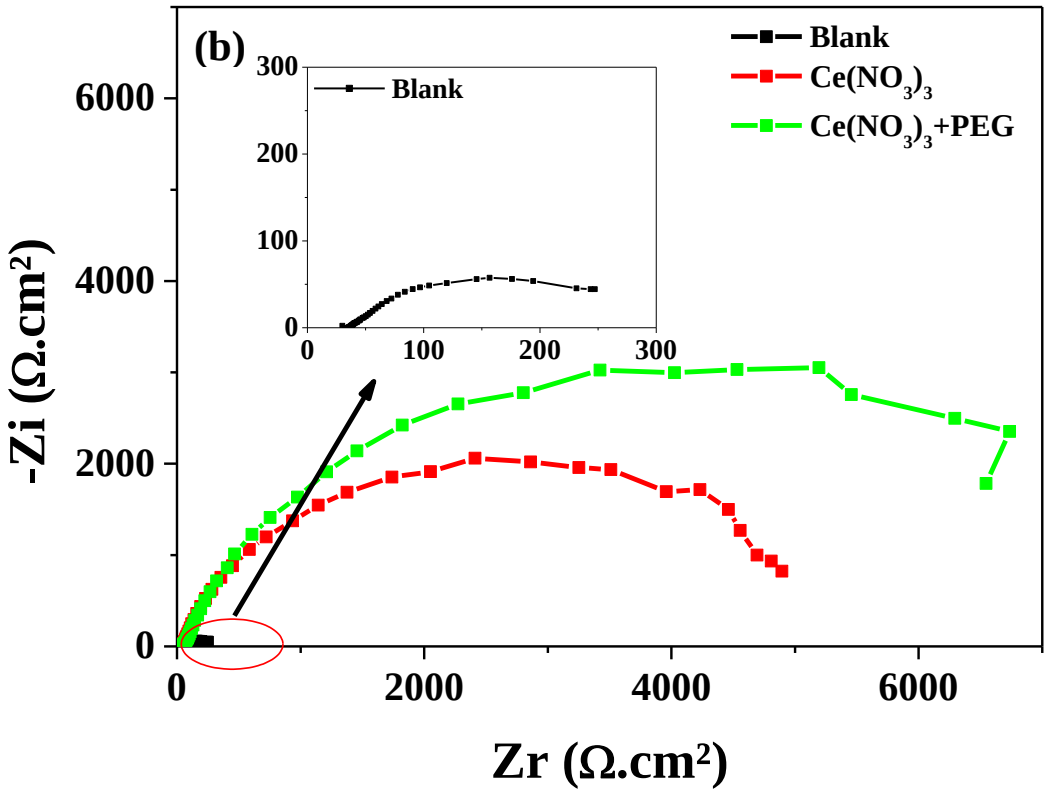
(b)
Blank
Ce(NO3)3
Ce(NO3)3+PEG
Blank
-Zi (Ω.cm²)
Zr (Ω.cm²)
0
2000
4000
6000
0
100
200
300

Figure 6b

Figure 7: SEM surface morphology of mild steel after (a) polished and (b) 30 min of immersion in 0.1M NaCl solution with the presence of 600 mg.L^{-1} of cerium nitrate, and PEG addition.

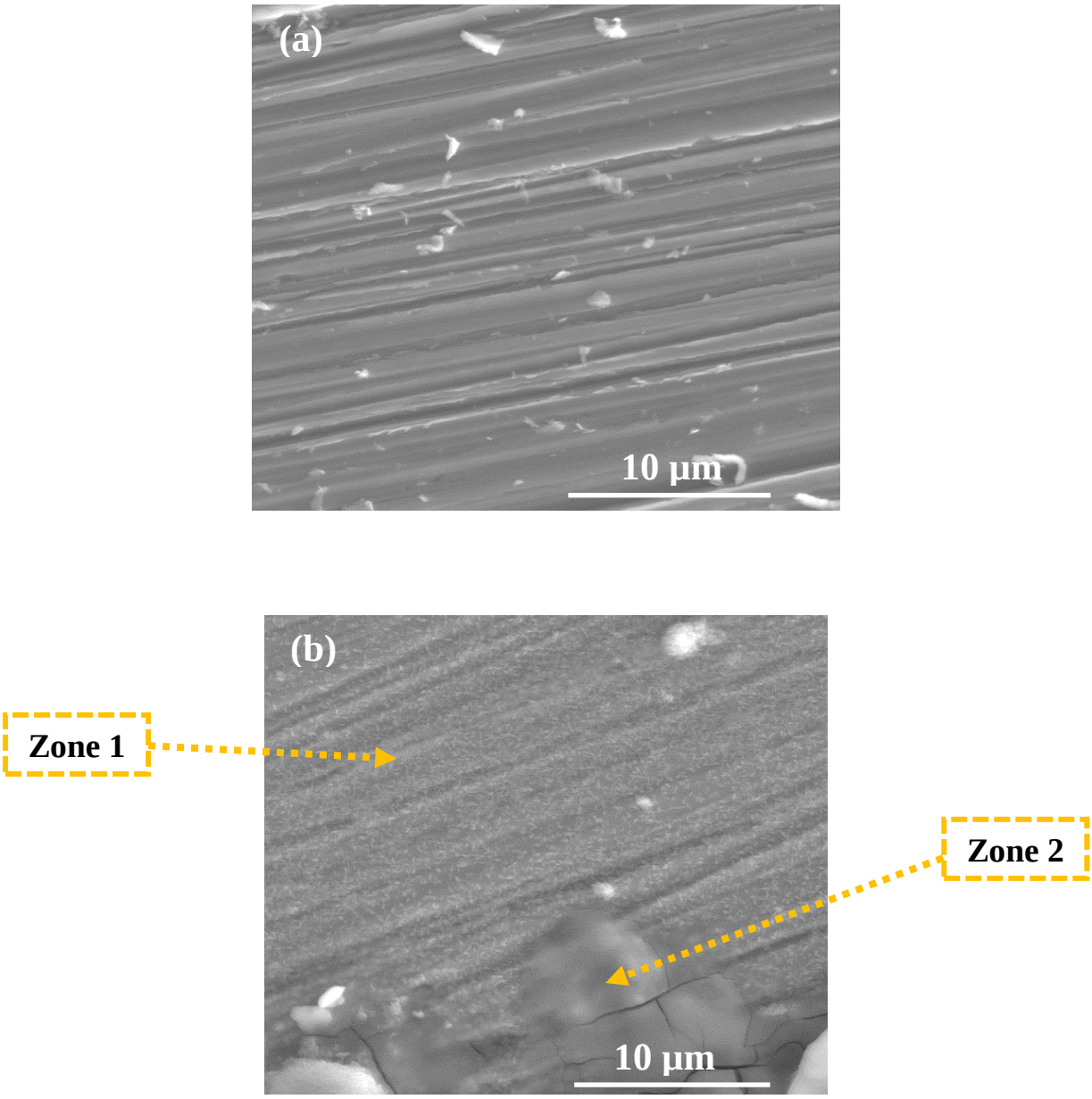

Figure 8: Evolution with time up to 30 days of (a) the polarization curves of Ce+PEG. (b) compares the polarization curves after 30 days of immersion in 0.1M NaCl of all the substrates.

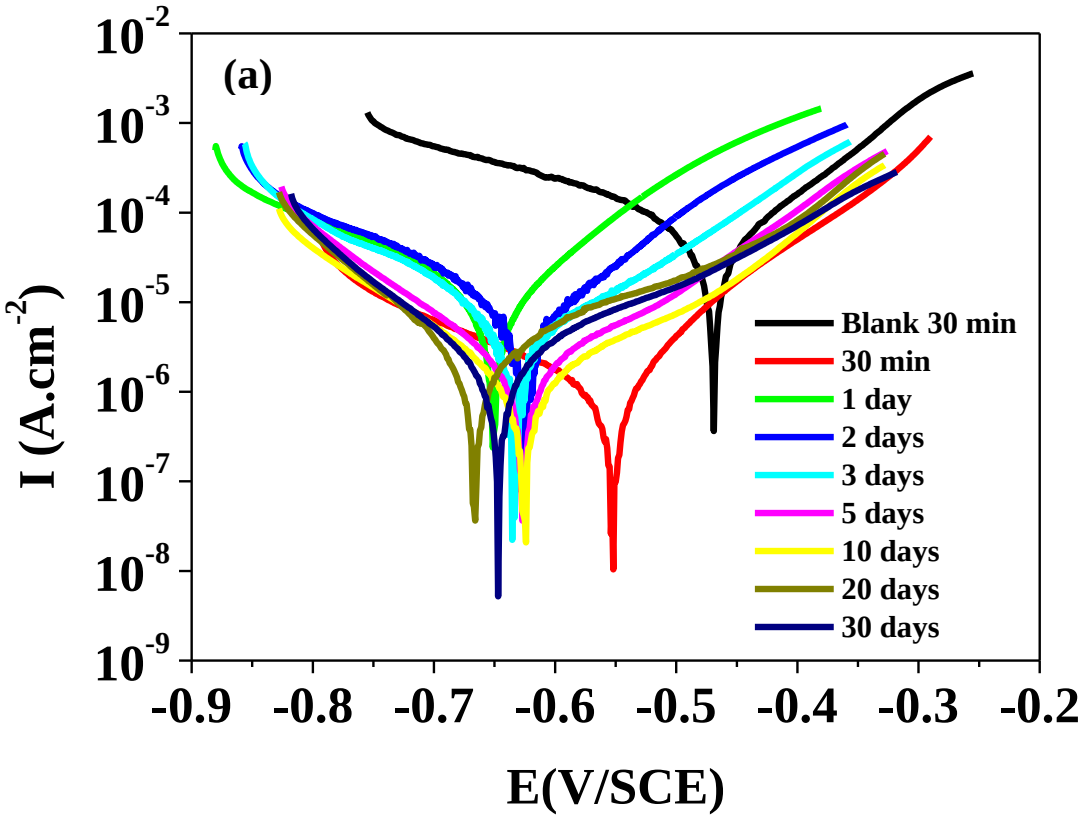

Figure 8a

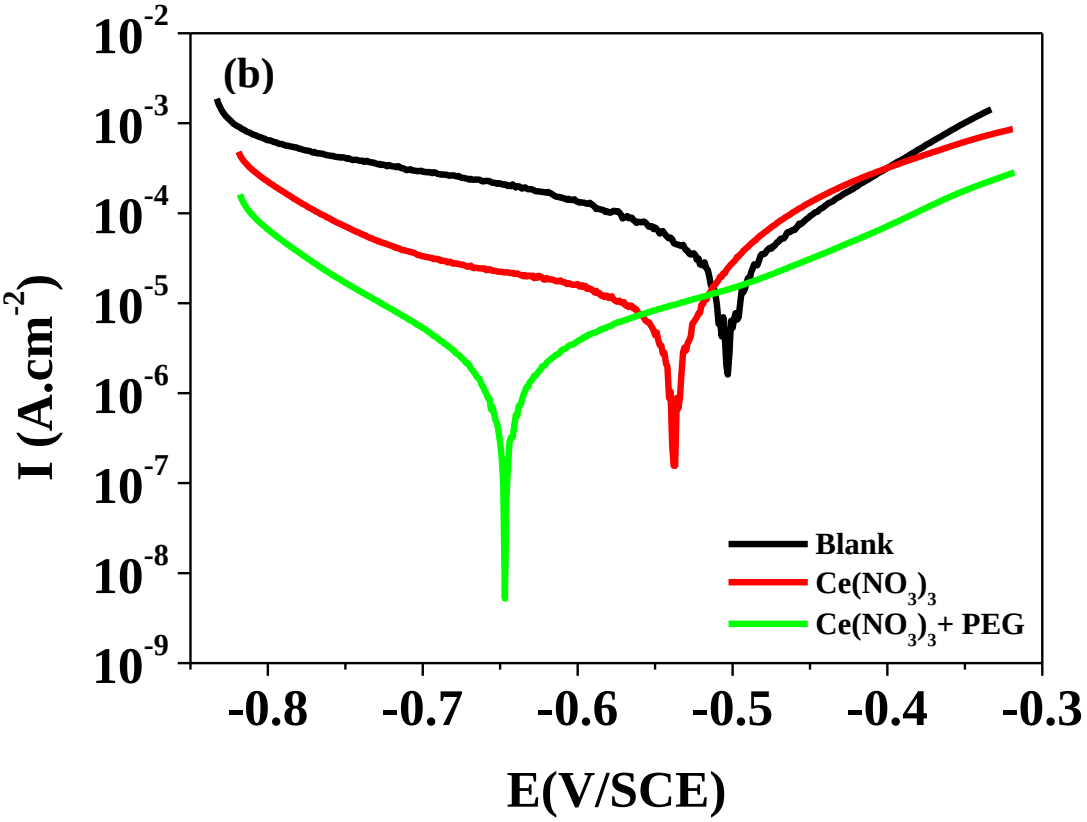
(b)
I (A.cm-2)
10-2
10-3
10-4
10-5
10-6
10-7
10-8
10-9
-0.8
-0.7
-0.6
-0.5
-0.4
-0.3
E(V/SCE)
Blank
Ce(NO3)3
Ce(NO3)3+ PEG

Figure 8b

Figure 9: EIS diagrams (Nyquist) recorded in 0.1M NaCl solution as function of immersion time for (a, b) bare mild steel; (c, d) with cerium nitrate inhibitor; (e, f) with PEG addition, after 30 days of immersion.

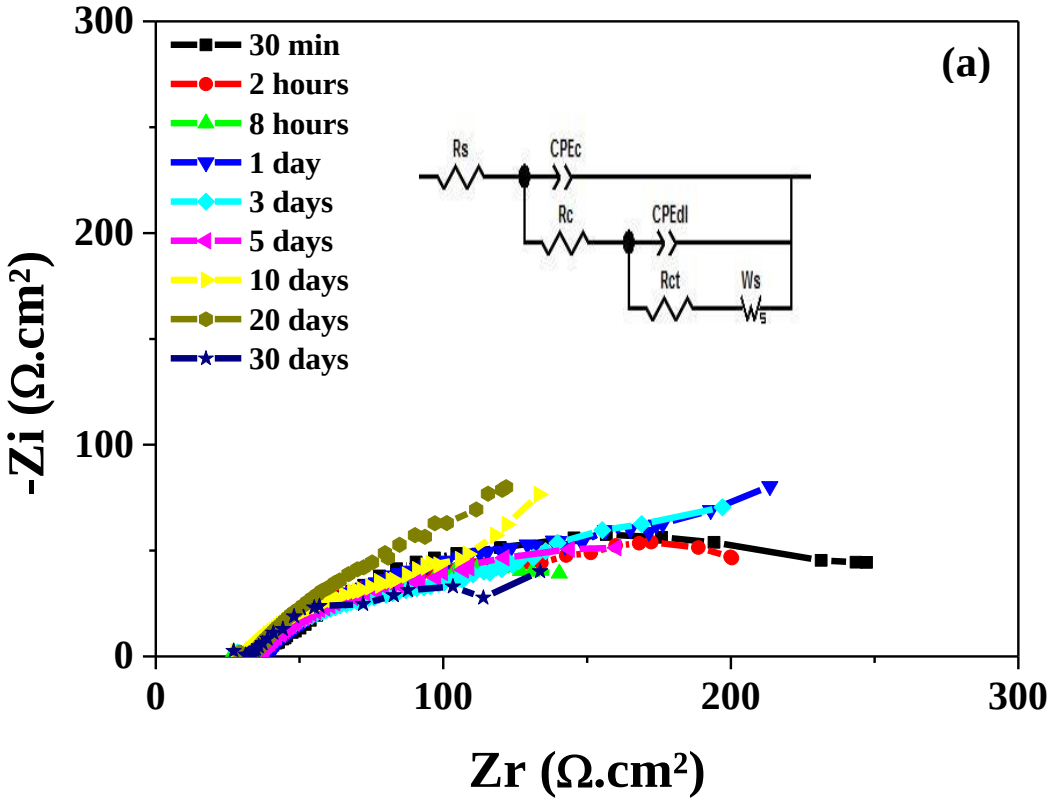

Figure 9a

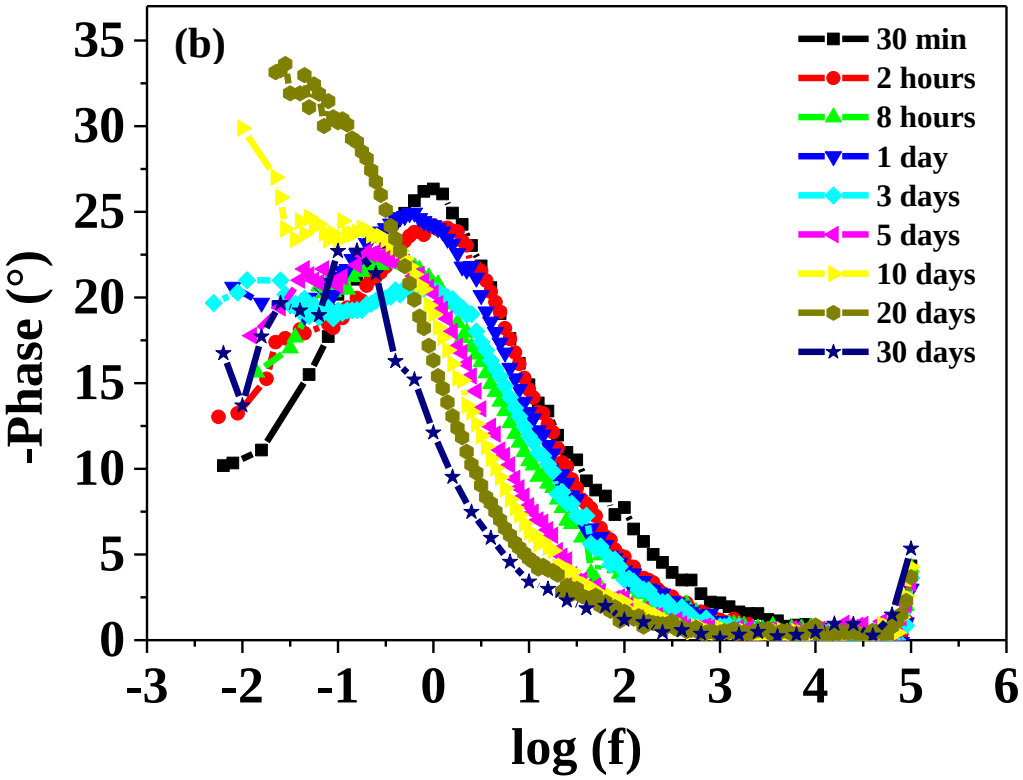
(b)
30 min
2 hours
8 hours
1 day
3 days
5 days
10 days
20 days
30 days
-Phase (°)
log (f)
35
30
25
20
15
10
5
0
-3
-2
-1
0
1
2
3
4
5
6

Figure 9b

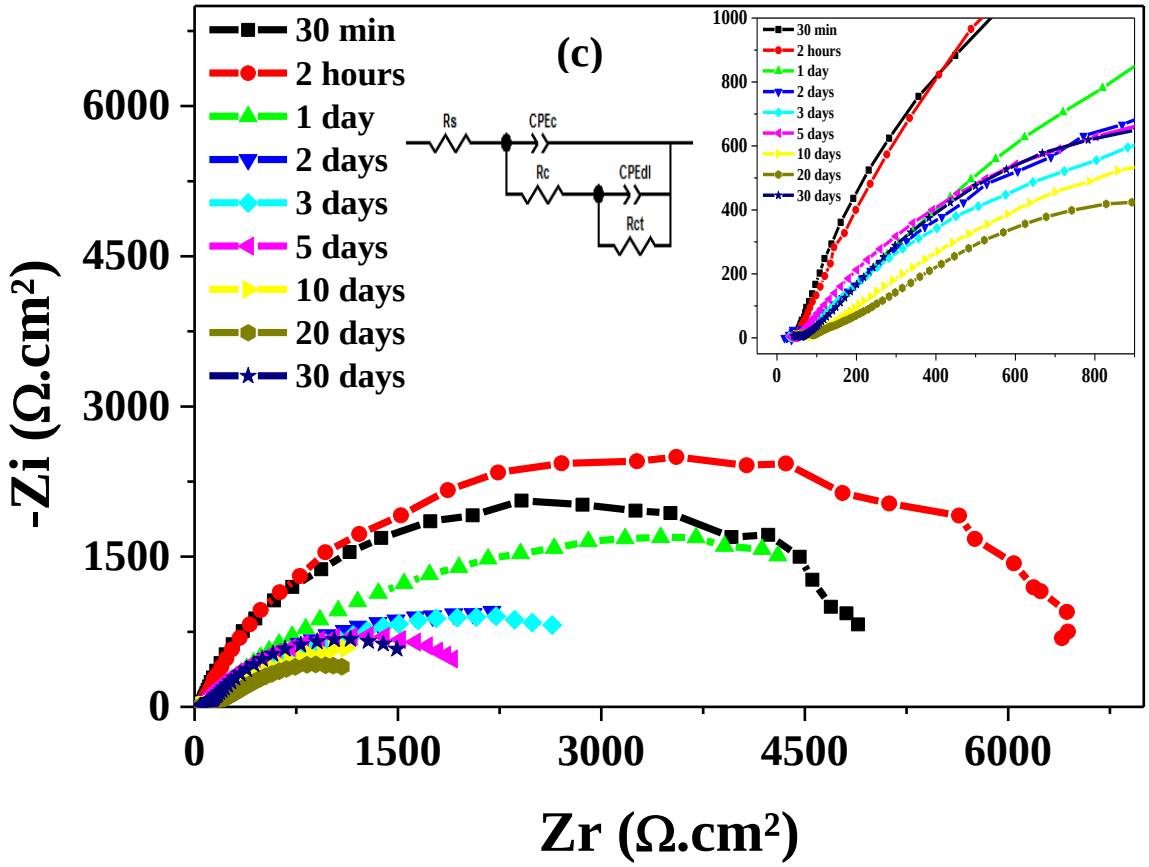
(c)
30 min
2 hours
1 day
2 days
3 days
5 days
10 days
20 days
30 days
Rs
CPEc
Rc
CPEdl
Rct
-Zi (Ω.cm²)
Zr (Ω.cm²)
0
1500
3000
4500
6000
200
400
600
800
1000

Figure 9c

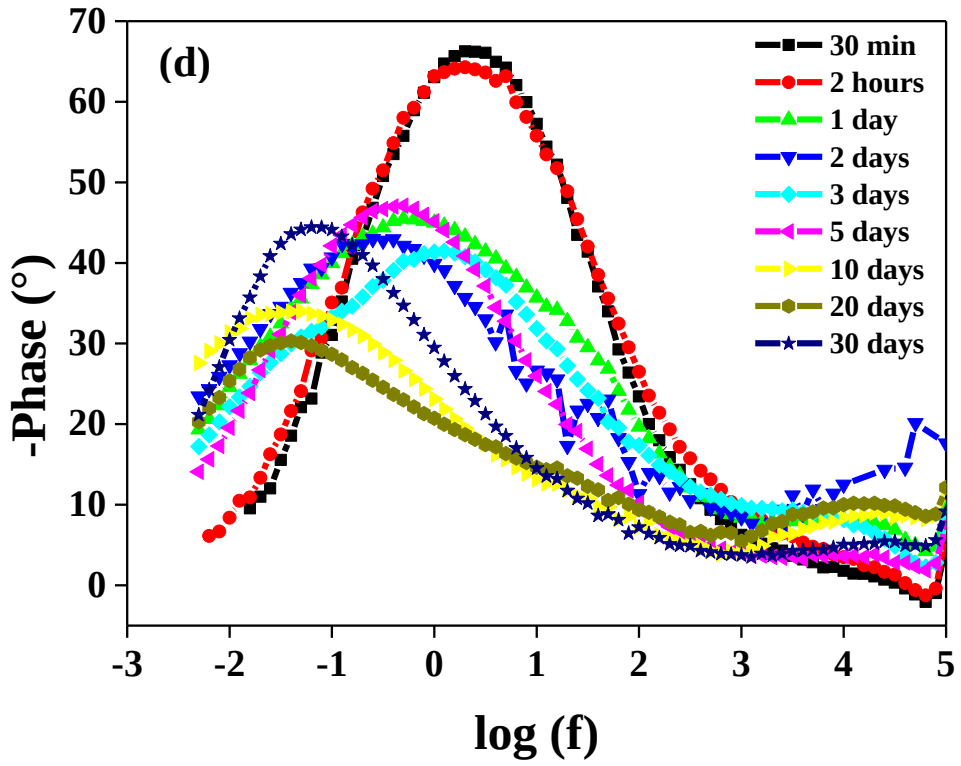
(d)
30 min
2 hours
1 day
2 days
3 days
5 days
10 days
20 days
30 days
-Phase (°)
log (f)
70
60
50
40
30
20
10
0
-3
-2
-1
0
1
2
3
4
5

Figure 9d

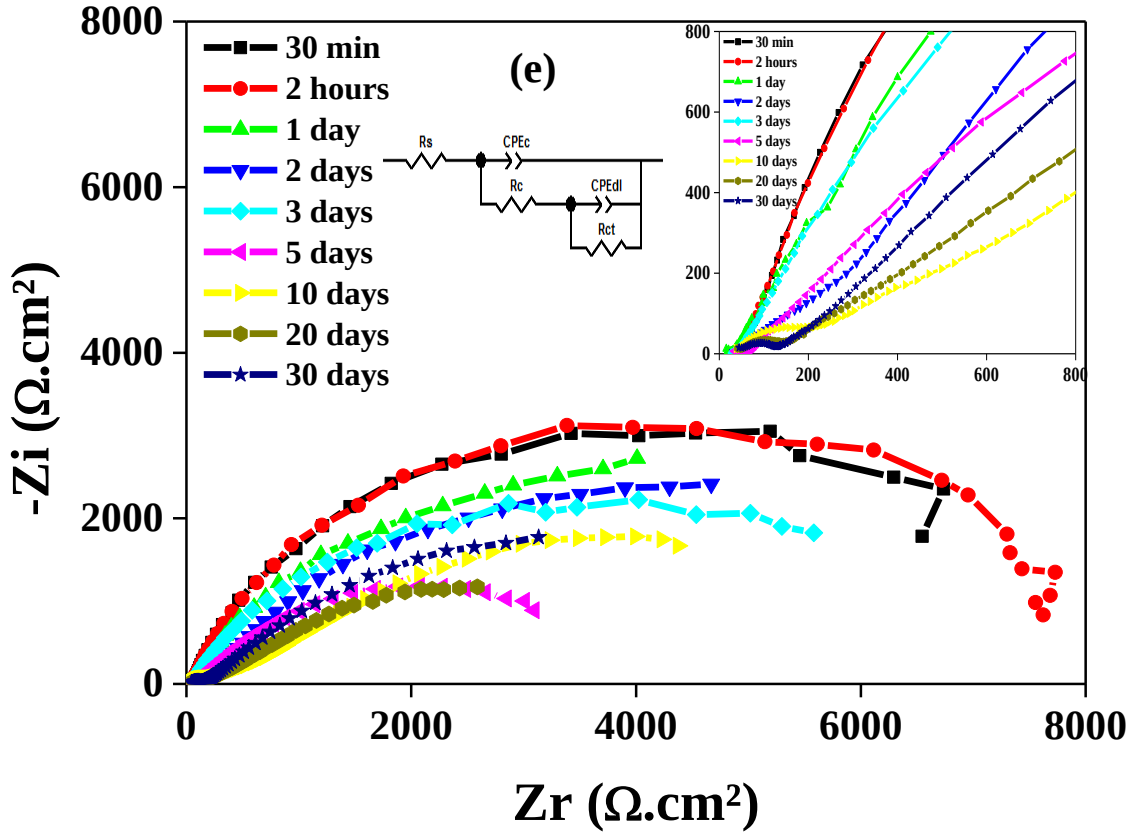
(e)
30 min
2 hours
1 day
2 days
3 days
5 days
10 days
20 days
30 days
Rs
CPEc
Rc
CPEdl
Rct
-Zi (Ω.cm²)
Zr (Ω.cm²)
0
2000
4000
6000
8000
200
400
600
800

Figure 9e

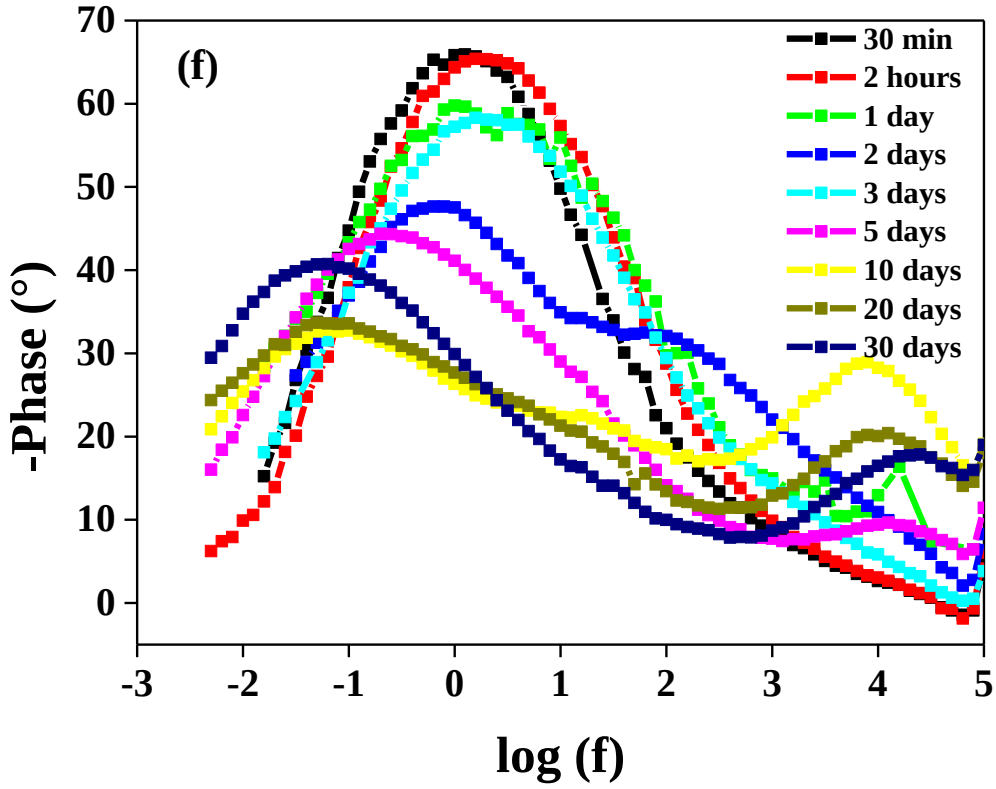
(f)
30 min
2 hours
1 day
2 days
3 days
5 days
10 days
20 days
30 days
-Phase (°)
log (f)
70
60
50
40
30
20
10
0
-3
-2
-1
0
1
2
3
4
5

Figure 9f

Figure 10: SEM images at different magnifications of the surface after 30 days of immersion in 0.1M NaCl (a, b) bare mild steel, (c, d) with cerium inhibitor and (e, f,) with addition of PEG addition. (g) is an EDS spectrum with PEG.

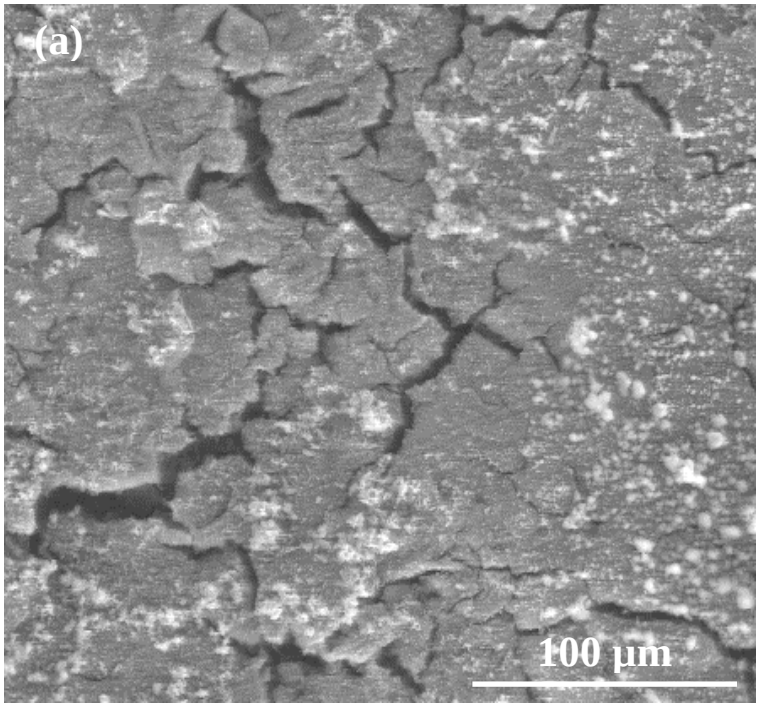

Figure 10a

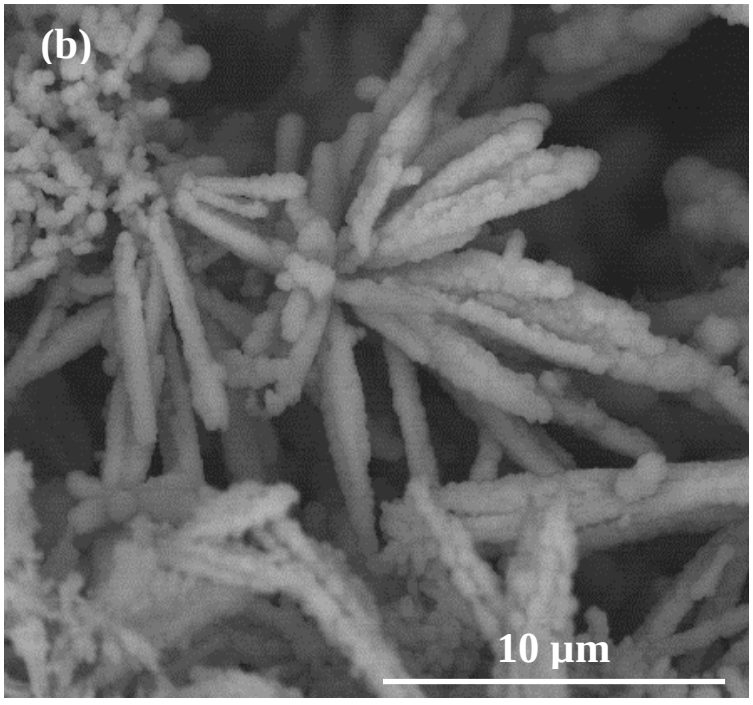

Figure 10b

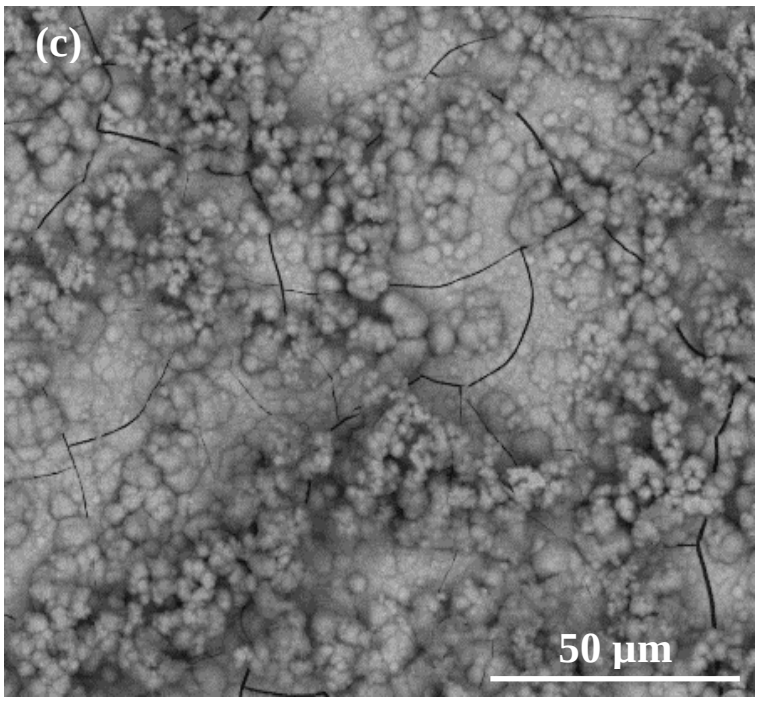

Figure 10c

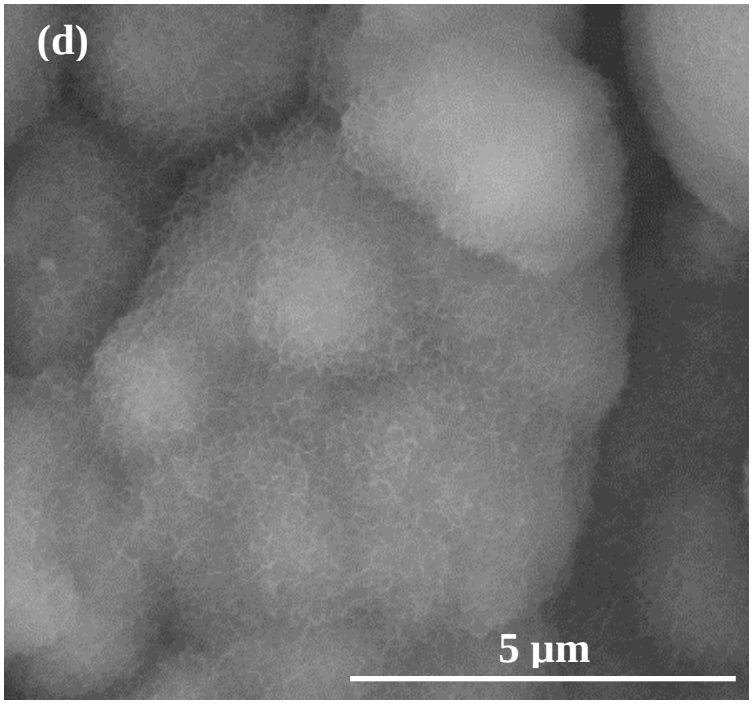

Figure 10d

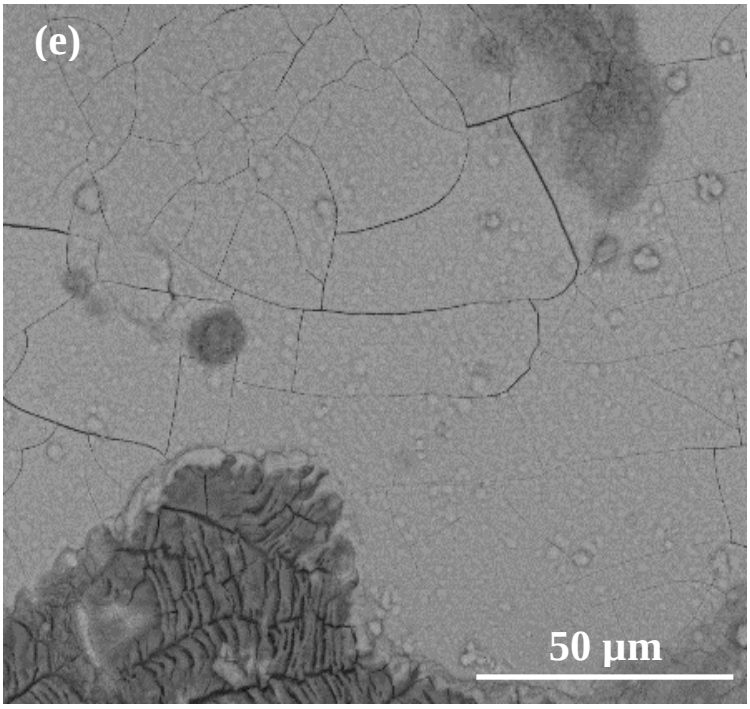

Figure 10e

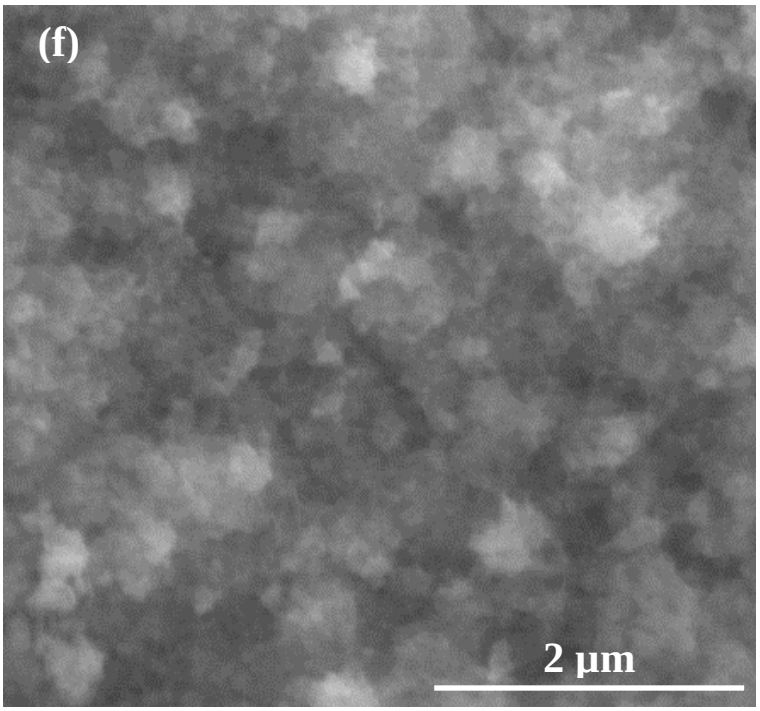

Figure 10f

(g)

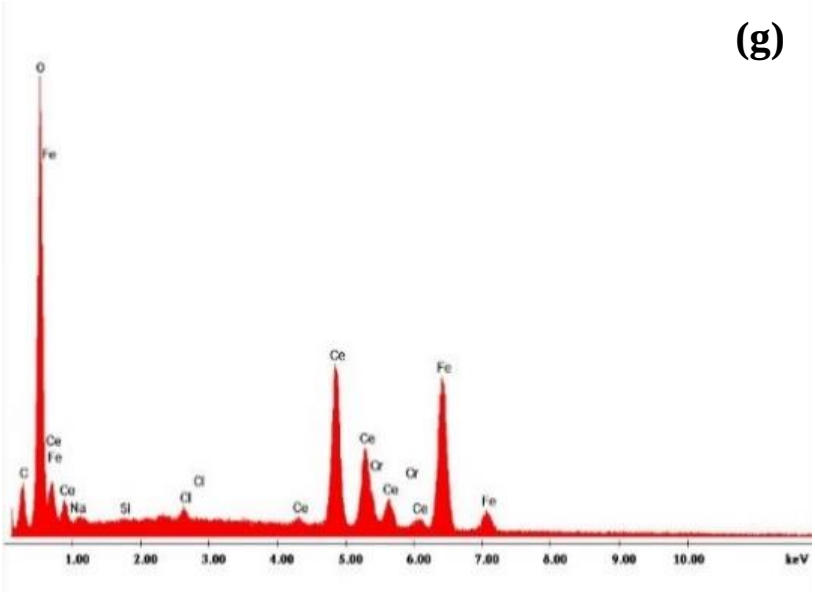
O
Fe
Ce
Fe
C
Co
Na
Si
Cl
Cl
Ce
Ce
Cr
Ce
Cr
Ce
Fe
Fe
1.00
2.00
3.00
4.00
5.00
6.00
7.00
8.00
9.00
10.00
keV

Figure 10g

Figure 11: Raman spectra of the films obtained with the presence of Ce+PEG in 0.1M NaCl solution as a function of immersion time up to 30 days.

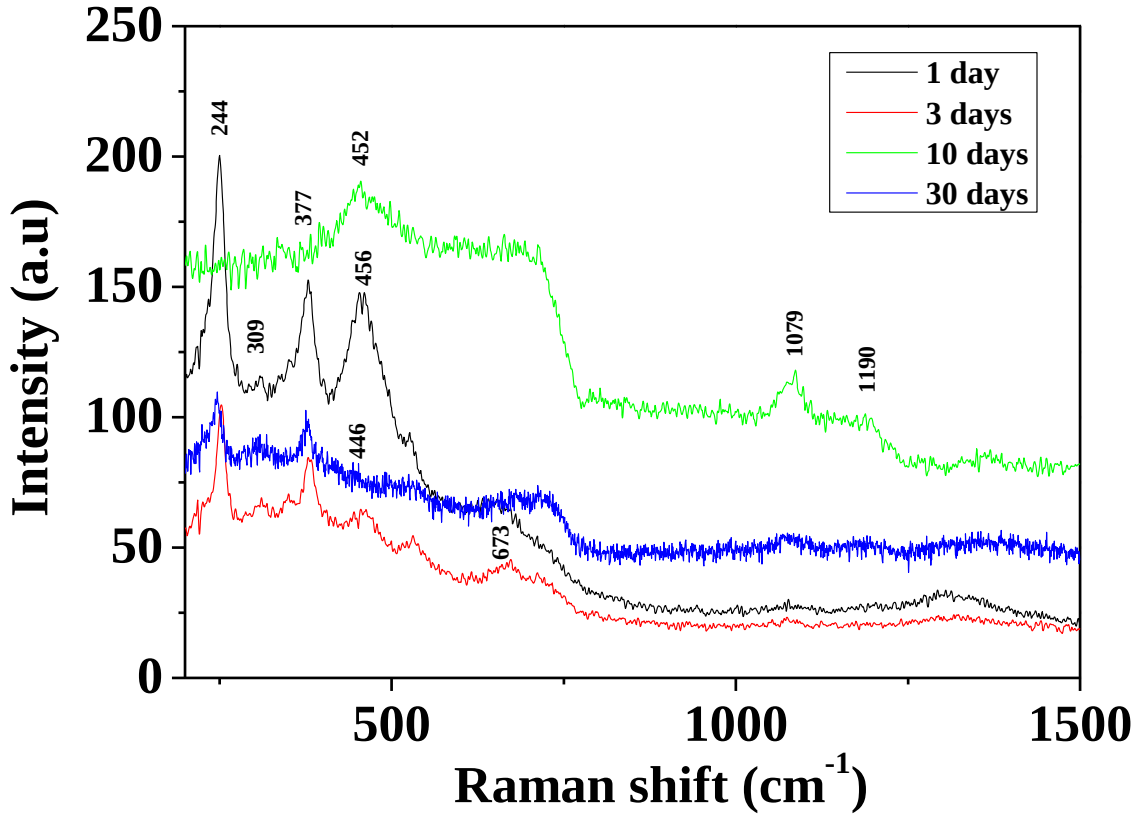

Figure 12: X-ray patterns of the films obtained with Ce+PEG addition after 30 days of immersion in 0.1M NaCl.

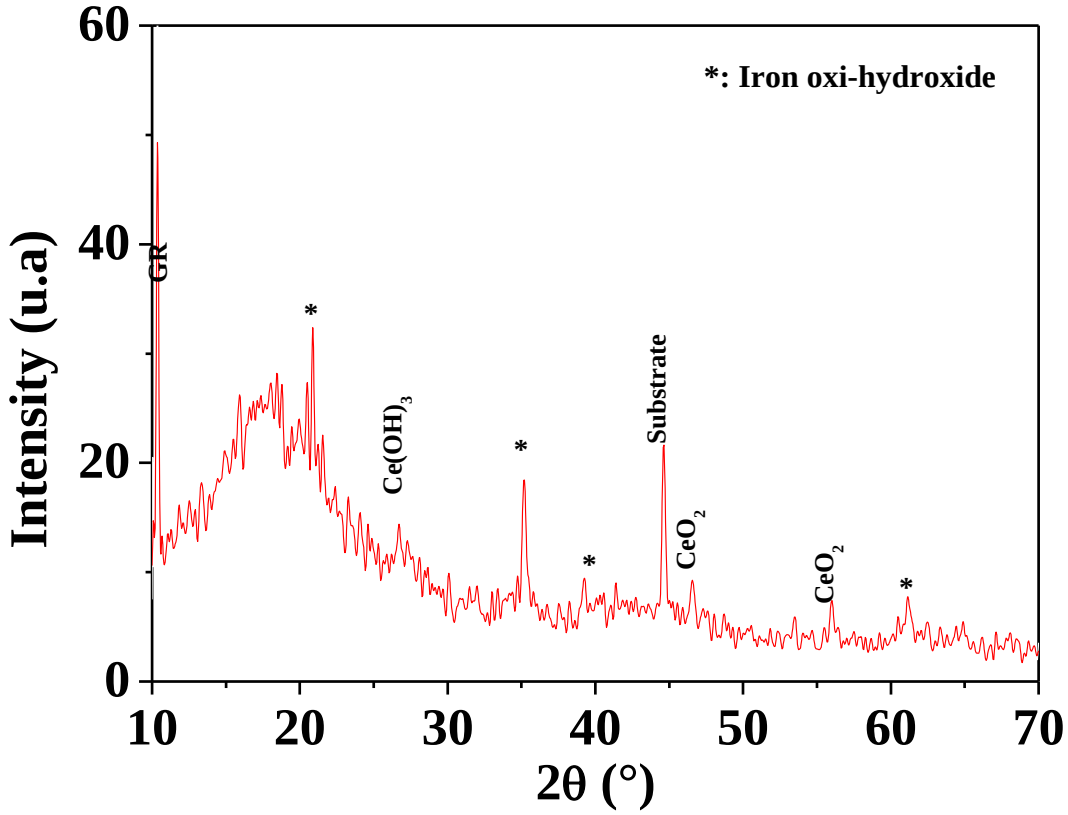

Figure 13: Raman spectra of the films obtained without and with PEG addition in 0.1M NaCl solution as a function of immersion time for 30 days.

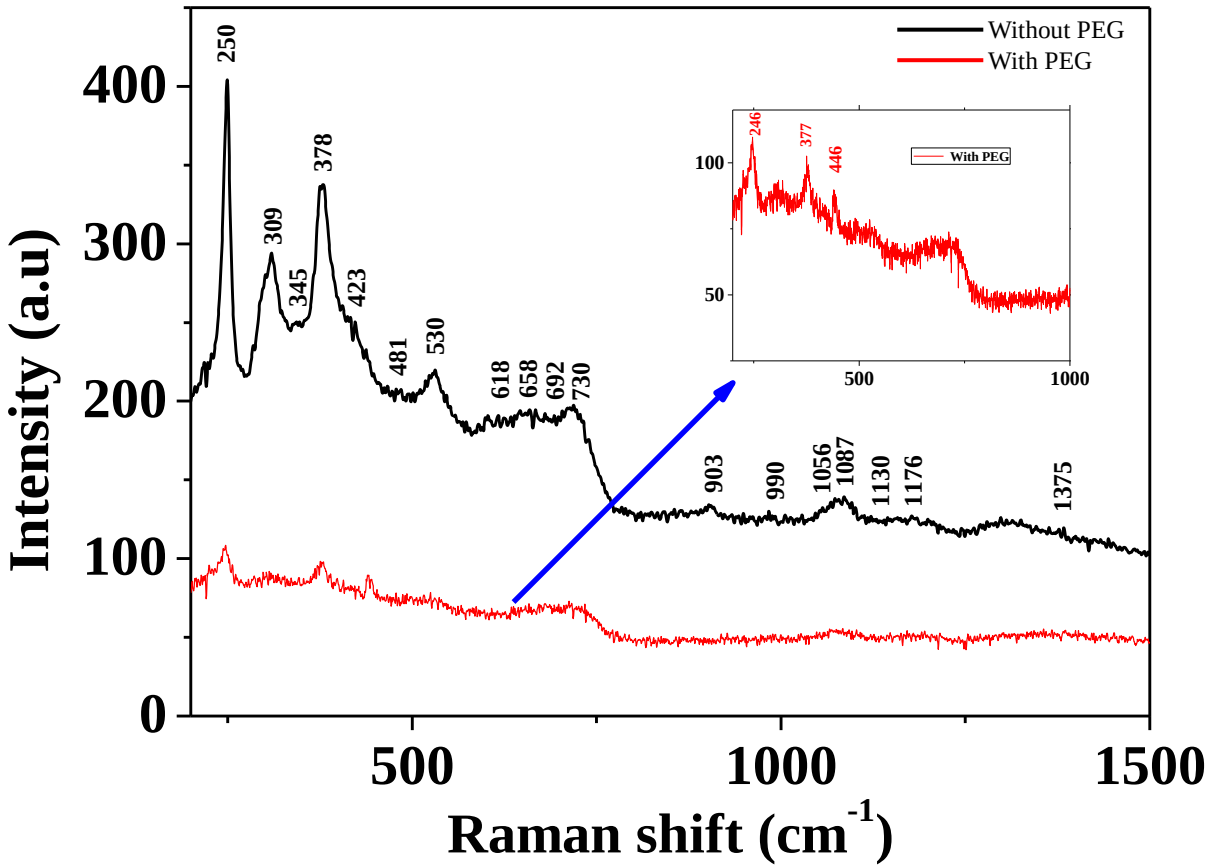

Table 1: Chemical composition (nominal) of ASTM A915 mild steel used in the tests (in wt.%)

C	Si	Mn	S	Cr	P	Al	V	Sn	Mo
0.33	0.24	0.65	0.024	1.06	0.017	0.007	0.022	0.001	0.015
W	**Ni**	**Cu**	**Co**	**Ti**	**Nb**	**B**	**Ta**	**Fe**	
0.256	0.003	0.088	0.001	0.001	0.003	0.002	0.014	rest	

Table 2: Electrochemical parameters calculated from polarization measurements on the mild steel electrode in 0.1 M NaCl solution with and without various concentrations of cerium nitrate at room temperature.

Concentration (mg/L)	**E_{corr} (mV/SCE)**	**βa (mV/dec)**	**βc (mV)**	**Rp (Ω.cm²)**	**I_{corr} (μA/cm²)**	**IE (%)**
Blank	- 468	111.0	261.1	227	148.90	-
50	- 522	126.2	164.5	419	74.40	50.03
100	- 551	72.8	206.7	2612	12.06	91.90
200	- 554	56.2	238.6	4998	5.17	96.52
400	- 565	62.5	179.4	5460	4.97	96.66
600	- 574	62.5	155.7	5919	4.59	96.91

Table 3: Fitting results for the EIS data of mild steel electrode with and without cerium nitrate inhibitor in 0.1M NaCl solution.

Concentration (mg/L)	**Rs (Ω cm^2)**	**n_c**	**CPE_c ($\mu F\ s^{(n-1)}\ cm^{-2}$)**	**R_c (Ω cm^2)**	**n_{dl}**	**CPE_{dl} ($\mu F\ s^{(n-1)}\ cm^{-2}$)**	**R_{ct} (Ω cm^2)**	**χ^2**
Blank	35.77	0.76	575	5	0.53	459	247	0.00119
50	38.05	0.62	918	17	0.89	800	455	0.00153
100	27.22	0.88	11	18	0.88	632	3455	0.00169
200	27.05	0.81	29	24	0.60	464	5035	0.00131
400	31.26	0.90	15	8	0.70	454	5140	0.00200
600	40.30	0.81	129	34	0.88	81.6	5229	0.00098

Table 4: Electrochemical parameters calculated from polarization measurements on the mild steel electrode with and without PEG addition after 30 minutes of immersion time in 0.1 M NaCl solution and at room temperature.

Composition	**E_{corr} (mV/SCE)**	**βa (mV/dec)**	**βc (mV)**	**Rp (Ω.cm^2)**	**I_{corr} (μA/cm^2)**	**IE (%)**
Blank	- 468	111.0	261.1	227	148.90	-
Ce	- 574	62.5	155.7	5919	4.59	96.91
Ce + PEG	- 561	73.9	173.6	8487	3.78	97.46

Table 5: Fitting results for the EIS data for mild steel electrode with and without PEG inhibitor addition in 0.1 M NaCl solution after 30 min of immersion time.

Composition	**Rs (Ω cm^2)**	**n_c**	**CPE_c ($\mu F\ s^{(n-1)}\ cm^{-2}$)**	**R_c (Ω cm^2)**	**n_{dl}**	**CPE_{dl} ($\mu F\ s^{(n-1)}\ cm^{-2}$)**	**R_{ct} (Ω cm^2)**
blank	35.77	0.76	575	5	0.53	459	247
Ce	40.30	0.81	129	34	0.88	81.6	5229
Ce + PEG	40.10	0.79	106.9	39	0.84	172.2	8082

Table 6: Electrochemical parameters of bare mild steel metal, with Ce and with (Ce + PEG) inhibitors at different immersion times.

Sample	Immersion time	E_{corr} (mV/SCE)	βa (mV/dec)	I_{corr} (μA/cm²)	IE (%)
Bare mild steel	0.5 h	- 468	111.0	148.90	-
	2 h	- 485	162.8	180.03	-
	8 h	- 534	160.8	198.97	-
	1 day	- 561	196.8	330.01	-
	3 days	- 583	211.6	362.55	-
	5 days	- 565	211.7	417.73	-
	10 days	- 595	195.5	563.35	-
	20 days	- 603	162.5	656.55	-
	30 days	- 503	114.9	427.41	-
Ce	0.5 h	- 574	62.5	4.59	96.91
	1 day	- 589	68.1	5.00	98.48
	2 days	- 655	108.8	17.69	94.95
	3 days	- 660	117.9	30.93	91.46
	5 days	- 673	135.6	37.98	90.90
	10 days	- 631	120.8	69.29	87.70
	20 days	- 609	157.7	85.59	86.96
	30 days	- 538	151.2	62.46	85.38
Ce + PEG	0.5 h	- 584	73.9	3.78	97.46
	1 day	- 651	88.8	4.74	98.56
	2 days	- 627	105.3	7.20	97.94
	3 days	- 635	110.5	6.51	98.20
	5 days	- 627	132.7	11.20	97.31
	10 days	- 624	154.6	14.47	97.43
	20 days	- 666	181.8	16.27	97.52
	30 days	- 647	158.6	13.45	96.85

Table 7: Fitting results for the EIS data of bare mild steel metal, with Ce and with Ce + PEG inhibitors at different immersion times.

Sample	time	Rs Ω cm^2	n_c	CPE_c $\mu F\ s^{(n-1)}\ cm^{-2}$	R_c Ω cm^2	n_{dl}	CPE_{dl} $\mu F\ s^{(n-1)}\ cm^{-2}$	R_{ct} Ω cm^2	W_{1-R} Ω cm^2	W_{1-T} Ω^{-1} cm^{-2}	W_{1-P}	χ^2
Bare mild steel	30 min	35.77	0.76	575	5	0.53	459	247	-	-	-	0.00119
	2 hours	32.95	0.63	561	9	0.69	918	210	-	-	-	0.00180
	8 hours	30.83	0.61	831	8	0.61	670	195	-	-	-	0.00129
	1 day	35.85	0.58	2639	9	0.63	864	120	560	2.89	0.38	0.00130
	3 days	33.35	0.61	2410	11	0.57	2350	110	520	2.37	0.38	0.00125
	5 days	34.58	0.55	1310	12	0.55	3230	87	275	1.20	0.47	0.00110
	10 days	30.86	0.61	4073	11	0.64	4385	71	1362	5.18	0.40	0.00190
	20 days	31.76	0.58	4805	10	0.65	4855	61	2170	6.88	0.37	0.00085
	30 days	30.49	0.63	1549	12	0.68	4809	75	510	2.25	0.45	0.00200
Ce	30 min	40.30	0.81	129	34	0.88	81.6	5229	-	-	-	0.00098
	2 hours	37.84	0.80	71.9	27.9	0.81	130.4	6778	-	-	-	0.00119
	1 day	40.91	0.84	34.2	20	0.58	634	5811	-	-	-	0.00084
	2 days	38.61	0.48	137.4	35.1	0.57	1402	4251	-	-	-	0.00127
	3 days	35.27	0.42	116.5	62.3	0.70	1162	4382	-	-	-	0.00074
	5 days	40.63	0.62	115.5	12.5	0.66	1305	2414	-	-	-	0.00108
	10 days	36.97	0.49	104	54.2	0.56	3886	2428	-	-	-	0.00200
	20 days	45.29	0.50	105	48.5	0.57	3113	1810	-	-	-	0.00172
	30 days	46.28	0.50	232	28.7	0.66	2790	2000	-	-	-	0.00159
Ce + PEG	30 min	40.10	0.79	106.9	39	0.84	172.2	8082	-	-	-	0.00104
	2 hours	37.20	0.80	75.8	33	0.81	114	8436	-	-	-	0.00082
	1 day	37.03	0.70	28.2	17	0.71	299	8100	-	-	-	0.00200
	2 day	39.15	0.55	192.7	60	0.82	108.7	7700	-	-	-	0.00067
	3 days	39.65	0.69	128.7	39	0.75	152.2	6850	-	-	-	0.00073
	5 days	36.72	0.59	47.7	34	0.59	342	5048	-	-	-	0.00172
	10 days	38.93	0.72	4.58	156	0.40	661	5610	-	-	-	0.00195
	20 days	46.26	0.74	3.80	94	0.43	1046	4840	-	-	-	0.00138
	30 days	39.25	0.55	22.7	109	0.53	1342	5350	-	-	-	0.00158

Table 8: Peaks for iron corrosion products using Raman spectroscopy shown in **figure 13**.

Corrosion product	**Peak (cm^{-1})**	**References**
Lepidocrocite (γ-FeOOH)	377-378, 658, 692, 1056-1067.	[41], [42]
Hematite (α-Fe_2O_3)	246-250, 286.	[41], [42]
Maghemite (γ-Fe_2O_3)	345-347, 1176-1190, 1375-1380.	[43], [44]
Goethite (α-FeOOH)	309, 481, 990, 1130.	[67], [68], [69]
Akaganeite (β-FeOOH)	730, 903.	[70]
Magnetite (Fe_3O_4)	666-673	[41], [71]
Iron hydroxychloride (β-$Fe_2(OH)_3Cl$)	423, 618.	[64]